

Pion-Hydrogen Phase Shift Analysis between 120 and 217 Mev

F. DE HOFFMANN, N. METROPOLIS, AND E. F. ALEI, *Los Alamos Scientific Laboratory, Los Alamos, New Mexico*

AND

H. A. BETHE, *Cornell University, Ithaca, New York*

(Received May 6, 1954)

An analysis has been made of the experimental angular distributions of negative pion—hydrogen scattering between 120 and 217 Mev. The usual assumptions of charge independence, and contributions from S and P waves only, are used and the six phase shifts determined as a function of energy by means of the Los Alamos MANIAC. The resulting phase shifts are used to predict positive pion—hydrogen scattering in this energy region. Comparison with the experimental data on positive pions enables one to exclude some of the sets of solutions obtained from the negative pion data.

Essentially three acceptable sets of solutions are found. Arguments are given why one of these is likely to be the physically correct one. Its characteristics are that the predominant phase angle with $T=3/2, j=3/2$ passes through 90° at about 195 Mev, that none of the other phase angles shows a resonance in our energy region, and that the $T=1/2$ phase angles are all small.

1. INTRODUCTION

IN the preceding paper Fermi and Metropolis¹ reported on an analysis of π meson-hydrogen scattering data in terms of phase shifts. The present paper continues to make the basic assumptions² used by Fermi and Metropolis that (a) nuclear forces are charge-independent and (b) only S and P waves contribute to the scattering. While the latter assumption is in some doubt³ we shall still make it for the sake of simplicity. Our analysis concerns the energy region between 120- and 217-Mev meson energy.

The experimental data (which are discussed more fully in Sec. 2, where references may also be found) consist of both transmission and angular distribution measurements. The total negative cross section (sum of the direct and charge exchange scattering⁴), $\sigma_T(\pi^-)$, is very well known from transmission measurements in our energy region. It shows a broad maximum from about 150 to 200 Mev (Fig. 1). The most recent transmission measurements of $\sigma_T(\pi^+)$ by the Carnegie Institute of Technology group also show a definite maximum in the same energy region and of the same shape but much higher in magnitude (Fig. 2). Older measurements, by both the Columbia and the Brookhaven groups, indicated considerably lower cross sections. However, the Carnegie transmission measurements are far superior in energy resolution and in statistical accuracy so that we propose to use them to the exclusion of the older measurements. The angular distributions for direct π^- and charge exchange scattering are fairly well established between 120 and 217 Mev. On

the other hand, the angular distribution of π^+ scattering is not known very well and we prefer to use it merely as confirmatory evidence, while considering the $\pi^- \rightarrow \pi^-$ and $\pi^- \rightarrow \pi^0$ angular distributions as primary data.

In principle the knowledge, at a given energy, of any two angular distributions (in our case $\pi^- \rightarrow \pi^-$ and $\pi^- \rightarrow \pi^0$) of the three scattering processes involved enables us to solve for the six phase shifts,⁵ $\alpha_3, \alpha_1, \alpha_{33}, \alpha_{31}, \alpha_{13}, \alpha_{11}$. However, as was anticipated, particularly by Ashkin and Vosko,⁶ and as we shall verify presently, there is actually a multiplicity of such sets of phase angles in our high-energy region. We shall find that some decision between solutions is possible on experimental grounds, but to a large extent we have to rely on theoretical discussions concerned with the physics of the situation.

The simplest physical argument concerns total cross sections. Both $\sigma_T(\pi^+)$ and $\sigma_T(\pi^-)$ show a maximum; of these, $\sigma_T(\pi^+)$ is especially suggestive of a resonance. Hence a solution which shows a resonance in the predominant phase angle would look more plausible than one that does not. Moreover, comparison of the recently

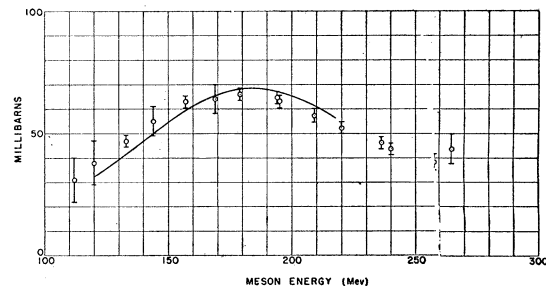


FIG. 1. The variation of $\sigma_T(\pi^-)$ —the sum of the total cross sections for direct and charge-exchange scattering of π^- from protons—versus energy. Only transmission measurements are shown. The curve is from interpolation (b) of Sec. 7.

¹ Fermi, Metropolis, and Alei, preceding paper [Phys. Rev. **95**, 1581 (1954)].

² H. L. Anderson *et al.*, Phys. Rev. **91**, 155 (1953).

³ M. Glicksman, Phys. Rev. **94**, 1335 (1954) has recently found that the angular distribution for $\pi^- \rightarrow \pi^-$ scattering at 217 Mev can best be fitted by including a fair amount of D wave in addition to S and P , although a reasonable fit is still obtained by S and P waves only.

⁴ The radiative absorption correction is negligible at our high energies.

⁵ Our phase shift designation is identical to that employed by Fermi and Metropolis in the preceding paper

⁶ J. Ashkin and S. H. Vosko, Phys. Rev. **91**, 1248 (1953).

obtained $\sigma_T(\pi^+)$ transmission data by the Carnegie group with $\sigma_T(\pi^-)$ shows that $\sigma_T(\pi^+) \approx 3\sigma_T(\pi^-)$ between 130 and 200 Mev; this suggests strongly, just as at the lower energy, that there is little contribution from the $T=\frac{1}{2}$ states. Next we argue that phase shifts which were small and well behaved at low energy will not suddenly become very large at higher energy; then α_{33} is the natural candidate for a resonance, and it also gives the correct magnitude for the resonance cross section.

Apart from the considerations just mentioned, we naturally prefer a solution which shows the smoothest and least steep variation of phase shifts. If necessary, in order to make a decision between solutions, we can also ask which of them resembles more closely the behavior to be expected from a purely theoretical strong-coupling calculation of phase shifts along the lines of the Tamm-Dancoff method.⁷

2. EXPERIMENTAL DATA⁸

a. Total Cross Section

The quantity $\sigma_T(\pi^-)$ has been well established, to about $\pm 2-3$ mb, between 133 and 258 Mev by transmission measurements at the Carnegie Institute of Technology.⁹ We show their values at 133, 157, 179, 194, 195, 215, 236, 240, and 258 Mev in Fig. 1. Also shown are selected transmission measurements of $\sigma_T(\pi^-)$ of the Chicago and Brookhaven groups. In particular the values are due to the following authors. At 112 Mev: Anderson *et al.*;¹⁰ 120 and 144 Mev: Anderson *et al.*;² 169 Mev: Fermi *et al.*;¹¹ 209 and 220 Mev: Glicksman;¹² 265 Mev: Yuan *et al.*¹³ It will be noted that the Brookhaven 265-Mev point appears somewhat out of line with the lower-energy data.

Good values for the positive cross section $\sigma_T(\pi^+)$ are available only from transmission measurements. Figure 2 indicates transmission measurements by means of a solid line and integration measurements by means of a broken line for the individual limits of errors. The transmission measurements are due to the following authors: at 110 Mev: Anderson *et al.*;² at 135, 152, 156, 166, 171, 185, and 196 Mev: Ashkin *et al.*;⁹ at 150, 180, 210, and 280 Mev: Yuan *et al.*¹³

Integration values are shown at 151, 188, and 225 Mev in Fig. 2. Those at 151 and 188 Mev are from photographic plate work; the 225-Mev measurement

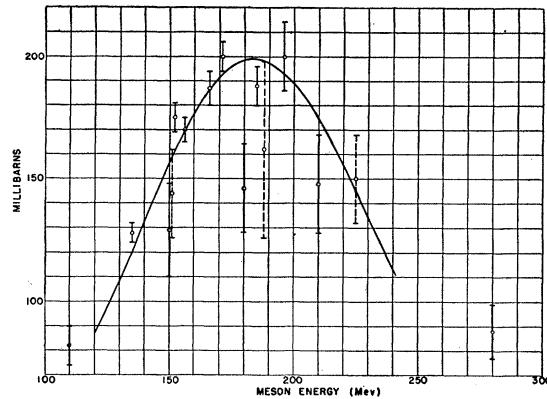


FIG. 2. The variation of $\sigma_T(\pi^+)$ —the total cross section of the scattering of π^+ from protons—versus energy. Experimental points shown by a solid line are transmission measurements, those shown by a dotted line are integration measurements. The curve is from interpolation (b) of Sec. 7.

was by means of a diffusion cloud chamber. The value at 151 Mev was obtained by Grandey and Clark¹⁴ by combining their data with those of Homa *et al.*,¹⁵ at that energy (a total of about 100 tracks). That at 188 Mev is due to Homa *et al.*¹⁵ (a total of about 40 tracks). The 225-Mev point, measured at Brookhaven, is due to Fowler *et al.*,¹⁶ and is based on 116 tracks.

Examining the $\sigma_T(\pi^+)$ measurements due to different experimenters we note that the results of Ashkin *et al.* have the greatest experimental accuracy. Not only is the statistical accuracy superior to the Brookhaven results, but also the energy definition is much better. In particular, it is about ± 6 Mev for the Carnegie experiments whereas it is about ± 25 Mev for the Brookhaven experiments. Thus, it is perhaps not too surprising that the Brookhaven transmission measurements miss the rather sharp maximum in $\sigma_T(\pi^+)$.¹⁷

An interesting comparison may be made between $\sigma_T(\pi^+)$ and $\sigma_T(\pi^-)$ as follows. It can easily be verified¹⁸ that

$$3\sigma_T(\pi^-) = \sigma_T(\pi^+) + 2\sigma_T(T=\frac{1}{2}), \quad (1)$$

where the last quantity in Eq. (1) denotes the scattering due to a pure state of isotopic spin $\frac{1}{2}$. Thus $3\sigma_T(\pi^-)$ is an upper limit to the value $\sigma_T(\pi^+)$ may reach. In actual fact, we see that the measured values of Ashkin reach this upper limit within experimental error. The Brookhaven measurement for $\sigma_T(\pi^+)$ is again exactly three times the value of $\sigma_T(\pi^-)$ as read off from Fig. 2. Thus we believe that $\sigma_T(T=\frac{1}{2})$ and hence α_1 , α_{13} , and α_{11}

⁷ G. F. Chew, Phys. Rev. 89, 591 (1953); and Dyson, Ross, Salpeter, Schweber, Sundaresan, Visscher, and Bethe, Phys. Rev. (to be published).

⁸ This section is not a complete survey of experimental data. In general only the most recent and more accurate results are quoted here.

⁹ Ashkin, Blaser, Feiner, Gorman, and Stern, private communication from J. Ashkin.

¹⁰ H. L. Anderson *et al.*, Phys. Rev. 85, 934 (1952).

¹¹ E. Fermi *et al.*, Phys. Rev. 92, 161 (1953).

¹² M. Glicksman, Phys. Rev. 94, 1335 (1954).

¹³ L. C. Yuan and S. J. Lindenbaum, Proceedings of the Fourth Annual Conference on High Energy Physics, Rochester (University of Rochester Press, Rochester, to be published).

¹⁴ R. A. Grandey and A. F. Clark, Phys. Rev. 94, 766 (1954).

¹⁵ Homa, Goldhaber, and Lederman, Phys. Rev. 93, 554 (1954), as corrected in a private communication to the authors.

¹⁶ W. B. Fowler *et al.*, Phys. Rev. 92, 832 (1953). The authors have recently corrected their reported mean energy from 260 Mev to 225 Mev.

¹⁷ L. C. L. Yuan, remark at the Fourth Annual Conference on High Energy Physics, Rochester (University of Rochester Press, Rochester, to be published).

¹⁸ See Eqs. (5)-(13).

TABLE I. Experimental data concerning the nine coefficients in Eqs. (2)-(4).

Mev	A_+	B_+	C_+
110	0.25±0.05	-0.34±0.06	0.53±0.14
135	0.35±0.20	-0.63±0.25	1.60±0.60
151	0.72 ^{+0.34} _{-0.27}	-0.36 ^{+0.28} _{-0.35}	1.46 ^{+0.93} _{-0.73}
188	1.32 ^{+0.93} _{-0.76}	-0.54 ^{+0.33} _{-0.44}	1.15 ^{+1.38} _{-0.56}
225	0.78	0.44	3.8

Mev	A_-	B_-	C_-	A_0	B_0	C_0
120	0.038±0.009	0.026±0.013	0.09±0.03	0.05±0.03	-0.15±0.04	0.25±0.13
144	0.09 ±0.02	0.08 ±0.03	0.17±0.05	0.12±0.05	-0.21±0.05	0.43±0.22
169	0.07 ±0.02	0.05 ±0.03	0.35±0.07	0.21±0.08	-0.07±0.07	0.49±0.26
194	0.15 ±0.03	0.09 ±0.05	0.39±0.11	0.23±0.11	-0.01±0.10	0.79±0.35
217	0.13 ±0.02	0.12 ±0.03	0.37±0.06	0.20±0.03	0.19±0.04	0.75±0.11

are small in our energy region, a fact we have already stressed in the introduction.

The Carnegie data enable one to draw a smooth curve from the maximum around 200 Mev to the Brookhaven values^{13,16} at 225 and 280 Mev and beyond. We have made use of this situation in our analysis.

b. Angular Distribution

Turning now to the differential cross section, we may write it, assuming only S and P waves, as¹⁹

$$\lambda^{-2}d\sigma(\pi^+\rightarrow\pi^+)/d\omega = A_+ + B_+ \cos\theta + C_+ \cos^2\theta, \quad (2)$$

$$\lambda^{-2}d\sigma(\pi^-\rightarrow\pi^-)/d\omega = A_- + B_- \cos\theta + C_- \cos^2\theta, \quad (3)$$

$$\lambda^{-2}d\sigma(\pi^-\rightarrow\pi^0)/d\omega = A_0 + B_0 \cos\theta + C_0 \cos^2\theta. \quad (4)$$

The available experimental data concerning the nine coefficients in Eqs. (2) through (4) are shown in Table I. The positive coefficients, A_+ , B_+ , C_+ , have been measured at 110 and 135 Mev by counter work at Chicago,² the measurements at 151 Mev,²⁰ 188 Mev¹⁵ are from photographic plate work, and that at 225 Mev²¹ was obtained by means of a diffusion cloud chamber. While the reported spread in energies is only ± 7 Mev at 151 Mev and ± 8 Mev at 188 Mev, the last point has an energy spread of ± 45 Mev. In addition, the Brookhaven data are not very well fitted by a formula of the type (2): either the point at 135° will fall below or that at 165° above the curve. If the latter is disregarded, a larger value of B_+ is indicated. In any case, the error in A_+ , B_+ , and C_+ at 225 Mev is quite large, just how large is difficult to estimate. Therefore, we give the 225-Mev values in Table I (and on Fig. 6) without showing limits of error.

The negative and zero coefficients of Eqs. (3) and (4) have been measured by counter work at Chicago. In particular the authors are, at 120 and 144 Mev:

¹⁹ In Eqs. (2) through (4) λ is the wavelength of the incident meson in the center-of-mass system.

²⁰ Combined results of Grandey and Clark (reference 14), and Homa *et al.* (reference 15).

²¹ W. B. Fowler *et al.* (reference 16). The resolution into A_+ , B_+ , C_+ was not performed by the Brookhaven group; therefore, the numbers quoted in Table I are our fit of Eq. (2) to the data.

Anderson *et al.*;² 169 and 194 Mev: Fermi *et al.*;¹¹ 217 Mev: Glicksman.¹² Of these, the 217-Mev point is the most recent and accurate one. One check on the accuracy is a comparison of the total cross sections: at 217 Mev one finds that integration of the Chicago differential measurements yields a total cross section for π^- of 56 mb, in excellent agreement with the Carnegie transmission value of 55.5 mb at 215 Mev. At 169 and 194 Mev on the other hand, the agreement between integration and transmission value is only good to about 10 percent.

3. METHOD

As noted in Sec. 2, the direct negative and charge exchange data are better known than the $\pi^+\rightarrow\pi^+$ data in our energy region. This has led us to a phase shift analysis in which we regard A_- , B_- , C_- , A_0 , B_0 , and C_0 as primary data; the six phase shifts are deduced and the resultant A_+ , B_+ , and C_+ are checked against the available positive pion data.

Before discussing the method proper, we list the formulas for the coefficients in terms of phase shifts for easy reference.²²

$$A_+ = \frac{1}{4}(|a|^2 + |c|^2), \quad (5)$$

$$B_+ = \frac{1}{4}(ab^* + a^*b), \quad (6)$$

$$C_+ = \frac{1}{4}(|b|^2 - |c|^2), \quad (7)$$

$$A_- = (1/9) \cdot \frac{1}{4}(|x|^2 + |z|^2), \quad (8)$$

$$B_- = (1/9) \cdot \frac{1}{4}(xy^* + x^*y), \quad (9)$$

$$C_- = (1/9) \cdot \frac{1}{4}(|y|^2 - |z|^2), \quad (10)$$

$$A_0 = (2/9) \cdot \frac{1}{4}(|p|^2 + |r|^2), \quad (11)$$

$$B_0 = (2/9) \cdot \frac{1}{4}(pq^* + p^*q), \quad (12)$$

$$C_0 = (2/9) \cdot \frac{1}{4}(|q|^2 - |r|^2), \quad (13)$$

²² In our notation the scattered amplitudes a , b , c , x , y , z , p , q , and r are lower case letters where Ashkin and Vosko (reference 6) use upper case letters. Conversely our coefficients in the angular distribution are denoted by upper case letters where they use lower case letters. Some authors (including the following paper by Martin) use a , b , c to denote $\lambda^2 A_+$, $\lambda^2 B_+$, and $\lambda^2 C_+$; we do not follow this practice but reserve these symbols for use as shown in Eqs. (5)-(7).

where²³

$$a = e^{2i\alpha_3} - 1, \tag{14}$$

$$b = 2e^{2i\alpha_{33}} + e^{2i\alpha_{31}} - 3, \tag{15}$$

$$c = e^{2i\alpha_{33}} - e^{2i\alpha_{31}}, \tag{16}$$

$$x = a + 2e^{2i\alpha_1} - 2, \tag{17}$$

$$y = b + 4e^{2i\alpha_{13}} + 2e^{2i\alpha_{11}} - 6, \tag{18}$$

$$z = c + 2e^{2i\alpha_{13}} - 2e^{2i\alpha_{11}}, \tag{19}$$

$$p = \frac{3}{2}a - \frac{1}{2}x, \tag{20}$$

$$q = \frac{3}{2}b - \frac{1}{2}y, \tag{21}$$

$$r = \frac{3}{2}c - \frac{1}{2}z. \tag{22}$$

Our method is in general similar to that used by Fermi and Metropolis for the work reported in the preceding paper. However, while they operate with nine differential cross sections (three for each of the three processes) we use the nine coefficients A, B, C in Eqs. (2)–(4). For details of the computer method we refer to the preceding paper.

In the present calculation the MANIAC is provided with the six input data A_-, B_-, C_-, A_0, B_0 and C_0 at a given energy, including the errors as shown in Table I. Each of these coefficients is dependent upon the six phase shifts as given in Eqs. (8)–(13). A given set of six starting phase angles is then varied by the MANIAC so as to minimize the least squares quantity,

$$M = \sum_{x=A_-, B_-, C_-, A_0, B_0, C_0} \left(\frac{x(\text{exp}) - x(\text{theor})}{\epsilon(x)} \right)^2. \tag{23}$$

Explicitly, in the first term in Eq. (23), $A_-(\text{exp})$ is the mean value of A_- as given in Table I, $A_-(\text{theor})$ the value obtained from Eq. (8) with a particular set of six phase angles, and $\epsilon(A_-)$ the experimental limit of error on A_- as given in Table I. If the result is $M=0$, then the corresponding phase angles solve our six equations exactly.

As has been pointed out repeatedly, particularly by Ashkin and Vosko,⁶ the system of Eqs. (8) through (13) has in general far more than one solution for one and the same set of six coefficients at a given energy. Thus the first task is to find all the solutions at a given energy resulting from the mean values of the six coefficients given in Table I. This is done by picking a random set of six phase angles (generated by the MANIAC) and asking the computer to minimize Eq. (23). Repeating this procedure many times will lead to a number of different solutions with M so close to zero that in essence these are the different solutions for one and the same set of A_-, B_-, C_-, A_0, B_0 , and C_0 .

After the different solutions at various energies have

²³ For $\pi^+ \rightarrow \pi^+$ scattering the nonspin flip amplitude is proportional to $(a+b \cos\theta)$, the spin flip amplitude to $c \sin\theta$. The other quantities are similarly the appropriate ones for $\pi^- \rightarrow \pi^-$ and $\pi^- \rightarrow \pi^0$ scattering.

TABLE II. Solutions at 217 Mev.

Solu- tion	α_3	α_1	α_{33}	α_{31}	α_{13}	α_{11}	A_+	B_+	C_+	$\sigma_T(\pi^+)$
1	20	4	73	14	-7	7	0.86	0.96	3.46	160
2	21	2	50	117	1	-1	0.98	0.92	3.35	167
3	-67	0	40	37	4	-11	0.85	0.93	3.51	161
4	19	6	35	73	-16	12	0.47	1.07	3.52	131
5	-2	15	125	-3	11	30	0.64	0.06	2.13	107
6	-65	0	165	-15	19	36	0.82	0.90	0.60	81

been found, we face the task of proper selection. The first criterion is the $\sigma_T(\pi^+) = 4\pi\lambda^2(A_+ + C_+)/3$ predicted by the solution. The second criterion is to compare the predicted A_+, B_+, C_+ of a solution with the experimental data, insofar as this is possible with the poorly known $\pi^+ \rightarrow \pi^+$ angular distributions.

4. SOLUTIONS AT INDIVIDUAL ENERGIES

a. Multiple Solutions at 217 Mev

Let us pick the 217-Mev point and examine the different solutions found. In Table II we exhibit the six solutions, and the resultant values of A_+, B_+, C_+ , and $\sigma_T(\pi^+)$. In all cases M [Eq. (23)] is low, so that all solutions arise from the same set of input coefficients, namely that given as the mean in Table I.²⁴

It should be pointed out that while the relative signs of the six phase shifts are fixed within each solution, all signs of a given solution can be reversed and the resulting solution will still satisfy Eqs. (8) through (13) and lead to identical values for A_+, B_+ , and C_+ . Moreover, any integral multiple of 180° can be added to any particular phase shift.

We should now like to make a selection between the solutions in Table II on the basis of the π^+ data. It is noted immediately that the first three solutions give nearly identical results also for π^+ scattering so that with any experimental accuracy now foreseeable for π^+ scattering, a distinction between these three will not be possible. The solutions 4, 5, and 6 differ substantially from solutions 1, 2, and 3 in the predicted π^+ scattering, both in total cross section and in angular distribution. From the available data on $\sigma_T(\pi^+)$ we can definitely exclude solutions 5 and 6 as giving too low values for $\sigma_T(\pi^+)$. We cannot be quite so definite about solution 4 because the lower limit of the experimental cross section at 225 Mev is just about 130 mb, the predicted cross section from solution 4. However, a smooth interpolation between the measured cross sections up to 200 and at 225 and 280 Mev indicates a value of about 160 mb at 217 Mev and thus makes solution 4 rather unlikely.

We now turn to the π^+ angular distributions predicted by our solutions 1 through 4. The resulting A_+, B_+ , and C_+ of solutions 1 through 3 are very close to each other. The comparison with the experimentally measured values may be seen by inspection of Table I

²⁴ In Sec. 6 we discuss to what extent the solutions are sensitive to changes of the input coefficients, within the limits of the experimental error on each listed in Table I.

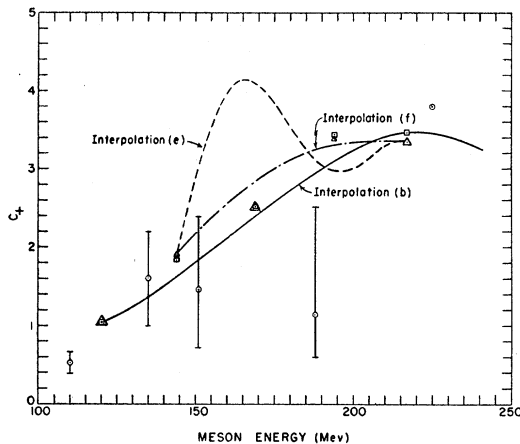


FIG. 3. The coefficient C_+ of Eq. (2) as a function of energy. The curves are interpolations discussed in Sec. 7.

and Fig. 3. A_+ of solutions 1 through 3 fits reasonably well with the experimental values of Table I. C_+ agrees within experimental error with the Brookhaven 225-Mev measurement, but the mean of the 188-Mev Columbia measurements is far out of line with any reasonable interpolation between our theoretical point (solutions 1 through 3) at 217 Mev and the lower-energy points. However, the very large limit of error of the 188-Mev Columbia point should be noted. The value of B_+ in solutions 1 to 3 seems high compared with the Brookhaven point at 225 Mev, and very high compared with the Columbia point at 188 Mev. However, it should be noted that if the 165° value of the Brookhaven data is disregarded, a larger value of B_+ is indicated at 225 Mev than we have chosen to give in Table I.

Note that solution 4 has a distinctly lower value of A_+ than solutions 1 through 3. In fact it seems quite low compared to the experimental evidence of Table I. We have already noted that solution 4 gives rather too low a value for $\sigma_T(\pi^+)$. Thus, while we cannot definitely exclude solution 4, we shall nevertheless choose to exclude it from our discussion because of its π^+ predictions.

The fact that A_+ , B_+ , and C_+ of solutions 1 through 3 are very close is a phenomenon which we shall find to be true of the groups of acceptable solutions at energies other than 217 Mev as well. This is confirmatory evidence for the statement made in the introduction that the $T=1/2$ contributions are not very important compared to the $T=3/2$ ones. Therefore, we believe that one can carry through much of the analysis by using the resulting A_+ , B_+ , and C_+ only. As a case in point, let us examine first why there are three acceptable solutions at 217 Mev.

For this purpose, it is very convenient to use the graphical method of Ashkin and Vosko²⁵ as applied to the π^+ angular distribution. In particular, we choose A_+ , B_+ , and C_+ of solution 1 and plot the Ashkin diagram. Then, as Ashkin and Vosko have pointed out,

we find two complex points a [Eq. (14)], which we denote by a_1 and a_2 . Ashkin has pointed out that in certain energy regions a_2 is excluded. The condition that a_2 is acceptable is that

$$|(a+b+3)-a| \leq 3. \quad (24)$$

The quantity $(a+b)$ is given by experiment. At 217 Mev one finds both a_1 and a_2 acceptable. Each of these points a leads both to a Fermi and a Yang solution (see Sec. 8, and Ashkin and Vosko⁶). By construction the point a_1 corresponds to $|\alpha_3| = 20^\circ$. One of the sets of α_{33} and α_{31} resulting from point a_1 is, again by *a priori* construction, solution 1. The other is roughly solution 2, as far as the $T=3/2$ phase shifts go. That it should not be exactly solution 2 is not surprising; after all, A_+ and C_+ of solution 2 do in fact differ slightly from that of solution 1. Putting it another way, solutions 1 and 2 could only be expected to be exactly corresponding Fermi and Yang type solutions if $\alpha_{13} = \alpha_{11} = 0$.²⁶

In the present case a_2 is exactly three units away from the point $(a+b+3)$; hence it just barely satisfies Eq. (24) and consequently leads to one and not two sets of α_{33} and α_{31} and thus to only one extra solution. In fact the solution it gives is very closely solution 3 of Table II as far as the $T=3/2$ phase shifts are concerned. Solution 3, it should be noted, is the same as the "first solution" found at 216 Mev by Fermi and Metropolis¹ during the summer of 1953.

b. Solutions at 120 and 144 Mev

At 144 Mev the computer found a total of seven distinct solutions. However, four of these resulted in values of $\sigma_T(\pi^+)$ in the range from 38 to 103 mb; we feel that these are excluded by the experimental data shown in Fig. 2. The other three solutions are given in Table III. Their $\sigma_T(\pi^+)$ seem acceptable, although that of solution 3 seems rather low. Of these solutions, 1 is of the Fermi type, and 2 and 3 are of the Yang type.

The question now arises how the solutions at 144 Mev are connected to solutions at another energy. In particular, we would like to connect the 144-Mev solutions with those at 120 Mev and those at 217 Mev (just discussed in Sec. 4a). One way of establishing some connection between solutions at different energies is the method of "tracking." By tracking between, say, 144 and 120 Mev we mean the following procedure: interpolate the six input coefficients *linearly* between 144 and 120 Mev in small energy steps (3 Mev in this

TABLE III. Solutions at 144 Mev.

Solution	α_3	α_1	α_{33}	α_{31}	α_{13}	α_{11}	A_+	B_+	C_+	$\sigma_T(\pi^+)$
1	-13	14	46	5	3	-5	0.49	-0.38	1.84	143
2	-12	12	21	60	-6	9	0.42	-0.36	1.91	136
3	-9	12	23	54	5	-16	0.29	-0.33	2.02	124

²⁵ See reference 6, and also Sec. 9 of this paper.

²⁶ This has been shown by H. A. Bethe (unpublished).

case). Then start the computer at 144 Mev with a particular set of angles corresponding to one of the solutions. The computer then finds a new set of phase angles at the energy $(144-\Delta E)$ Mev to fit the six linearly interpolated input coefficients. Eventually 120 Mev is reached in this fashion. We are fully aware that physically a linear interpolation of the input coefficients need not be correct. In actual fact, however, it is likely to be not too far from the truth in the energy region from 120 to 144 Mev since the experimental data seem rather smooth. In any case we believe that, while intermediate energy results should not be trusted, the procedure of "tracking" does provide an insight into which solutions are related at 120 and 144 Mev. The tracking procedure is not likely to be as good when applied from 144 Mev upward in energy since there is little reason to believe that the six input coefficients vary linearly over energy intervals as large as 25 Mev in this region.

As to actual results of the tracking between 144 and 120 Mev, we find that all three solutions of Table III track vary smoothly, with M very small at all intermediate energies, down to 120 Mev. The resulting values at 120 Mev are shown in Table IV. It is seen that the π^+ data deduced from solution 3 are significantly different from those obtained from solutions 1 and 2 which agree between themselves. In the first place, solution 3 gives a value for $\sigma_T(\pi^+)$ which appears too low in comparison with Fig. 2. But much more striking is the discrepancy of A_+ ; the directly measured values at 110 and 135 Mev interpolate to give $A_+ \approx 0.27$ at 120 Mev which is compatible with $A_+ = 0.20$ as deduced from solutions 1 and 2 but certainly not with $A_+ = 0.04$ deduced from solution 3. Hence solution 3 is excluded at 120 Mev and by continuity, therefore, we also reject solution 3 at 144 Mev. Solutions 1 and 2 at 120 Mev are both acceptable in terms of the resulting π^+ data; solution 1 is the Fermi and 2 the Yang type. Note that we have assigned the over-all signs of the phase shifts such that α_3 is negative and α_1 is positive. This agrees with the choice of sign necessitated by the extensive low-energy experiments between 40 and 78 Mev.²⁷ Hence there is no ambiguity in over-all sign at 120 or 144 Mev.

Thus we are led to believe that at 144 Mev only solutions 1 and 2 of Table III are acceptable. Just as at 217 Mev, the two solutions which we accept at 144 Mev have almost identical A_+ , B_+ , and C_+ . To understand this more fully, it is advisable to draw an Ashkin

TABLE IV. Solutions at 120 Mev.

Solu- tion	α_3	α_1	α_{33}	α_{31}	α_{13}	α_{11}	A_+	B_+	C_+	$\sigma_T(\pi^+)$
1	-12	8	30	6	2	-4	0.20	-0.36	1.04	87
2	-12	8	14	37	-3	4	0.20	-0.36	1.05	87
3	-11	8	20	24	5	-13	0.04	-0.35	1.19	69

²⁷ For a detailed discussion of these see the forthcoming book, *Mesons and Fields*, Vol. II, by H. A. Bethe and F. de Hoffmann.

TABLE V. Solutions at 169 Mev.

Solu- tion	α_3	α_1	α_{33}	α_{31}	α_{13}	α_{11}	A_+	B_+	C_+	$\sigma_T(\pi^+)$
1	-4	7	64	3	-1	7	0.77	-0.11	2.53	177
2	-4	7	32	96	0	6	0.78	-0.11	2.52	174
3	-42	7	49	12	1	2	0.81	-0.12	2.50	176
4	-3	9	32	88	-4	10	0.69	-0.08	2.64	168
5	-2	6	58	10	-8	14	0.54	-0.04	2.78	156

diagram from the A_+ , B_+ , C_+ of, say, solution 1. We then find that now only one of the complex points a [Eq. (14)] is acceptable, *viz.*, a_1 . The other, as Ashkin and Vosko have pointed out, is unacceptable because the inequality Eq. (24) is violated. The acceptable a leads to two sets of P phase shifts for $T = \frac{3}{2}$, one of which is by construction identical to solution 1 (Fermi solution) while the other is very close to solution 2 (Yang solution).

c. Solutions at 169 and 194 Mev

The solutions at 169 and 194 Mev were again obtained by starting from different random sets of angles, as described in Sec. b. The method of "tracking" described in Sec. 4b was used to obtain the connection of sets at different energies, and also turned up some additional solutions.²⁸ For instance, solution 3 of Table II was tracked starting at 217 Mev and led to a solution at 194 Mev not previously found by the random angle method.

By these means solutions at 169 Mev were found; the acceptable one as far as π^+ predictions are concerned are tabulated in Table V. At 169 Mev we rejected the three other solutions found which yielded $\sigma_T(\pi^+)$ between 77 and 126 mb.²⁹ All solutions given in Table V have an M value close to zero. As explained in Sec. 3, the MANIAC computes A_- , B_- , C_- , A_0 , B_0 , and C_0 from the six phase angles of the particular solution and compares them with the mean experimental values quoted in Table I. Hence, M close to zero means that A_- , B_- , C_- , A_0 , B_0 , and C_0 given by the solution are essentially identical with the mean experimental values.

Table VI gives the "acceptable" solutions at 194 Mev. We rejected one solution which yielded $\sigma_T(\pi^+) = 124$ mb. We might also reject solutions 7 and 8 as giving too low $\sigma_T(\pi^+)$. This time it should be noted that all but solutions 2 and 3 have M values not close to zero; in particular all other solutions give C_0 about 0.76 instead of 0.79 as given in Table I (of course, this is well within the experimental error) while the other input coefficients do correspond to the mean values of

²⁸ This method was also used at 144 and 217 Mev to ascertain that the maximum acceptable solutions are found.

²⁹ Even the accepted five solutions give lower values for $\sigma_T(\pi^+)$ than the transmission values, 190-200 mb, of the Carnegie Institute of Technology group. Also the $\sigma_T(\pi^-)$ obtained by integration of the 169-Mev differential cross sections is too low. This may throw some doubt on the accuracy of the 169-Mev results at least as far as absolute values are concerned.

TABLE VI. Solutions at 194 Mev.

Solu- tion	α_3	α_1	α_{33}	α_{31}	α_{13}	α_{11}	A_+	B_+	C_+	$\sigma_T(\pi^+)$
1	-13	-14	94	-14	1	8	0.96	0.39	3.43	191
2	-22	7	67	143	-4	-11	1.08	0.40	3.31	199
3	-43	1	58	23	5	-19	0.80	0.25	3.81	189
4	-13	-14	82	-22	-1	2	0.99	0.23	3.46	195
5	-13	-14	86	-13	0	3	0.99	0.28	3.46	195
6	14	15	60	133	-4	-2	0.97	0.43	3.39	192
7	16	17	30	74	-22	4	0.55	0.84	2.92	139
8	13	14	33	72	-22	9	0.46	0.67	3.19	140

Table I. Note how many acceptable solutions exist at 194 Mev; we shall have occasion to understand how critical an energy region this is in Sec. 5. This leads us to believe, for instance, that the differences between solutions 7 and 8 are not truly significant, and also those between solutions 1, 4, and 5.

5. CONNECTION OF SOLUTIONS AT DIFFERENT ENERGIES

The most difficult task is to decide which solutions at a certain energy are in reality connected to solutions at another energy. The first attempt in this direction is our method of "tracking" (Sec. 4b) with the input coefficients linearly interpolated between two energies at which measurements have been made. We should emphasize again that in fact there is no reason for the coefficients to vary linearly between, say, 169 and 194 Mev. However, if the phase shifts vary smoothly on a track from one energy to another, then we believe this to give an indication of a likely connection. This linear tracking indicates the existence of the following apparent tracks:

Track T1: Solution 1 at all energies.

Track T1a: Same as Track T1, except Solution 5 at 194 Mev.

Track T2: Solution 3 at 120 Mev and 144 Mev, Solution 2 at 169 Mev, Solution 6 at 194 Mev, Solution 2 at 217 Mev.

Track T3: Solution 3 at 169 Mev, 194 Mev, and 217 Mev.

Track T4: Solution 2 at 120 Mev and 144 Mev, Solution 4 at 169 Mev, Solution 7 at 194 Mev, Solution 4 at 217 Mev.

Let us now examine the behavior of the phase angles as a function of energy for Track T1. In particular we focus our attention on the biggest phase shift, namely, α_{33} . We notice that between 120 and 194 Mev α_{33} rises smoothly from 30° to 94° . However, at 217 Mev solution 1 of Table II gives $\alpha_{33}=73^\circ$, which reverses the smooth upward trend of the curve. However, we are at liberty to reverse the sign of all angles in solution 1 at 217 Mev and to add 180° where desirable. In this way, we can replace α_{33} by $\alpha_{33}'=180-73=107^\circ$, so that now α_{33} continues to rise smoothly up to 217 Mev. This modification has the advantage that the reversal of sign of the other angles also makes them fit better to the lower energy results.

There is, however, one difficulty; if we actually track from solution 1 at 194 Mev to solution 1 at 217 Mev by the method described, then the relative signs as given in Tables II and VI are definitely specified; in particular, α_3 which starts at a negative value goes through zero and then becomes positive. The question arises why the solution of opposite sign is not found by the MANIAC. The explanation may be given most easily in terms of the behavior of the point a on an Ashkin graph of the positive coefficients.

The first steps in construction of the Ashkin diagram are the determination of $|a+b|$ from the forward scattering and $\text{Re}(a+b)$ from the total cross section. This means that the point $(a+b)$ is determined in the complex plane except for the sign of its imaginary part. Now it can easily be verified from Eqs. (14) and (15) that

$$\text{Im}(a+b) = \sin 2\alpha_3 + 2 \sin 2\alpha_{33} + \sin 2\alpha_{31}. \quad (25)$$

Thus, at energies below 120 Mev the quantity $\text{Im}(a+b)$ is seen to be positive and the point $(a+b)$ must be chosen in the upper half of the complex plane. (This in turn determines the sign of α_3 which will result from the construction of the Ashkin diagram.³⁰) Now assume that there is in fact a resonance in α_{33} , i.e., this quantity passes through 90° , and assume further that the other two phase shifts are small (as indeed they are for Track T1). Then expression (25) has to change sign and becomes negative above the resonance; the imaginary part of $(a+b)$ has to go through zero at some energy. Now, experimentally, this imaginary part is determined from the difference, D , of the squares of $|a+b|$ and $\text{Re}(a+b)$,

$$D = \text{Im}^2(a+b) = |a+b|^2 - [\text{Re}(a+b)]^2, \quad (26)$$

or

$$\frac{1}{4}D = (A_+ + B_+ + C_+) - (A_+ + \frac{1}{3}C_+)^2. \quad (27)$$

Both terms on the right of Eq. (27) are large quantities compared to D near the point where D itself is close to zero. Now the two quantities on the right are obtained from interpolation of inaccurate experimental data at any given energy. Hence, it is very unlikely that D goes *exactly* to zero at a given energy with input values used in the MANIAC. It is possible that D will either go negative when the energy is increased by a certain energy step and remain negative for a certain energy range or else D remains positive all the time. In the former case there is then no solution at all in the interval in which D is negative; in the latter case the imaginary part never goes exactly through zero. With the actual observations (interpolated) the latter is realized; in fact, the lowest value of D is about

$$D \approx 0.006(a+b)^2. \quad (28)$$

The computer following the experimental values of D

³⁰ Choosing the other point $(a+b)$ thus simply reverses the sign of α_3 as obtained from the graph.

has no opportunity to reverse the sign of $\text{Im}(a+b)$ and therefore keeps this imaginary part positive.

A "mistake" in the imaginary part of $(a+b)$ is equivalent to a reversal of sign of all phase shifts. Hence, above the resonance the computer will give the incorrect sign for all α 's.

Now in actual fact the primary input data into the MANIAC are not the positive but the negative and zero coefficients. The argument can be rephrased easily in terms of these. The relevant Ashkin diagram then involves x [Eq. (17)] and y [Eq. (18)]. The quantity which is analogous to D is then given by

$$D' = |x+y|^2 - [\text{Re}(x+y)]^2. \quad (29)$$

Since we find that in our energy region the $T = \frac{1}{2}$ phase shifts are small, the quantities x and y are not very different from a and b . Therefore, just as in the positive case, Eq. (29) has difficulty in going through zero and the argument carries through in the same way.

These considerations show that the phase shifts near 194 Mev are extremely sensitive to the experimental data. The sensitivity is further increased if α_{11} and α_{13} are also permitted to be different from zero. Thus, the multiplicity of solutions found in this critical energy region is not very surprising.

Based on this sensitivity at 194 Mev, we decided in particular not to distinguish between Track T1 and T1a, which are identical except for a small difference around 194 Mev. Instead we shall henceforth speak of a Track I, where an average of solutions 1 and 5 of Table VI is chosen at 194 Mev and where the signs at 217 Mev are reversed as discussed and as indicated in Table VII. A track of type T1 has been found independently by Glicksman¹² who made an analysis under the assumption that $\alpha_{31} = \alpha_{13} = \alpha_{11} = 0$.

Examining Tracks T2 and T4 with respect to overall consistency, we note that Track T2 starts with an unacceptably low $\sigma_T(\pi^+)$ at 144 Mev and ends up with a very acceptable $\sigma_T(\pi^+)$ at 217 Mev. On the contrary, Track T4 starts with a very acceptable solution at 144 Mev and ends up with a somewhat low cross section at 217 Mev. Closer examination of the entire behavior of the two tracks shows that the respective phase angles come very close together in the intermediate energy region. Therefore the connection between the high and low energy end is not clearly established and a slightly different interpolation of $A_-, B_-, C_-, A_0, B_0,$ and C_0 may easily lead to a different result.

TABLE VII. Track I.

Energy (Mev)	α_3	α_1	α_{33}	α_{31}	α_{13}	α_{11}
217	-20	-4	107	-14	7	-7
194	-13	-14	90	-16	0	5
169	-4	7	64	3	-1	7
144	-13	14	46	5	3	-5
120	-12	8	30	6	2	-4

TABLE VIII. Tracks II and IIa.

Energy (Mev)	Track II					
	α_3	α_1	α_{33}	α_{31}	α_{13}	α_{11}
217	-21	-2	130	243	-1	1
194	-22	7	67	143	-4	-11
169	-4	7	32	96	0	6
144	-12	12	21	60	-6	9
120	-12	8	14	37	-3	4

Energy (Mev)	Track IIa					
	α_3	α_1	α_{33}	α_{31}	α_{13}	α_{11}
217	21	2	50	117	1	-1
194	14	15	60	133	-4	-2

We have, therefore, switched the connection at 169 Mev. Furthermore, at 194 Mev solutions 2 and 6 are very similar with regard to the large phase shifts α_{33} and α_{31} and with regard to A_+, B_+, C_+ . Hence we consider solution 2 equally acceptable as solution 6. We therefore adopt a Track II which uses solution 2 at all energies except that at 194 Mev it may use either solution 2 or 6.

At low energies Track II is the Yang solution. As will be shown in Sec. 8, the Yang solution which is the counterpart of the Fermi solution represented by Track I is characterized by a very rapid increase of the phase shifts, particularly of α_{31} in the neighborhood of 200 Mev. Being the counterpart of Track I, it yields an α_3 whose behavior is essentially the same as for Track I. Therefore we choose at 217 Mev to reverse the signs of all phase shifts of solution 2 in Table II. Since this makes $\alpha_3 = -21$ at 217 Mev and $\alpha_3 = -4$ at 169 Mev, we find that now solution 2 at 194 Mev fits in better than solution 6, and we therefore select it. Then, in order to maintain a monotonic increase of α_{33} and α_{31} , we add 180° to the former and 360° to the latter to the values quoted in Table II with signs reversed. This yields the data listed in Table VIII for Track II.

The very rapid increase of α_{33} from 169 to 217 Mev is apparent, and the increase of α_{31} is even more rapid. It is evident, however, that the interpolation from 169 Mev up and the choice of signs and multiples of 180° is to a large extent arbitrary for Track II. It would be entirely possible to choose a less rapid increase of the phase shifts, for instance as shown in Track IIa in Table VIII in which we have chosen solution 6 at 194 Mev, chosen the signs at 217 Mev as in solution 2 of Table II, and omitted the addition of multiples of 180° . From 169 Mev down, Track IIa agrees with Track II. Unlike II, Track IIa shows a maximum in both α_{33} and α_{31} instead of a monotonic increase.

It will be noted that T3 "disappears" below 169 Mev. In fact, performing the linear tracking between 169 and 144 Mev, the track seems to disappear at about 146 Mev. The detailed behavior is indicated in Table IX. At 169 Mev Track T3 has a value $M = 1 \times 10^{-5}$, i.e., the solution reproduces the mean input

TABLE IX. Disappearance of track T3.

Mev	A_-	A_0	B_-	B_0	C_-	C_0	α_2	α_1	α_{33}	α_{31}	α_{13}	α_{11}
149	0.086	0.174	0.069	-0.191	0.210	0.462	49	-10	-36	-19	-3	8
147	0.088	0.173	0.069	-0.204	0.197	0.453	47	-10	-36	-17	-3	8
145	0.089	0.124	0.079	-0.205	0.177	0.431	14	-12	-47	-5	-2	5
144	0.090	0.120	0.080	-0.210	0.170	0.430	14	-12	-46	-5	-2	6

Mev	A_+	B_+	C_+	M	$\sigma_T(\pi^+)$	$\sigma_T(\pi^-)$
149	0.645	-0.365	2.10	3×10^{-2}	167	60
147	0.636	-0.403	2.04	5×10^{-2}	165	60
145	0.512	-0.372	1.87	1×10^{-4}	145	53
144	0.494	-0.380	1.83	4×10^{-7}	142	53

coefficients essentially exactly. As the energy is lowered, all six phase angles vary smoothly towards their values at 147 Mev shown in Table IX. However, the value of M rises very sharply until it reaches a value of 5×10^{-2} at 147 Mev. Between 147 and 145 Mev there is a sharply discontinuous behavior. This is evidenced most strikingly in the phase angles. At the same time, the value of M has become very much lower again and at 144 Mev essentially solution 1 of Table III is reached. We believe that this behavior indicates that in actual fact Track T3 disappears. What seems to happen as we approach 147 Mev from above is that the computer has to use a set of A_- , B_- , C_- , A_0 , B_0 , and C_0 more and more different from the interpolated input coefficients in order to find a solution of type T3. Finally the M becomes so high that the minimum disappears and then the computer is forced to look for another "type" of solution at that energy. It searches around for a considerable length of time (this is physically indicated by the comparative length of time it takes to go from 147 to 145 Mev as compared to from 149 to 147 Mev) and finally falls into another track, namely, Track T1.³¹

The variation with energy of the principal phase shifts is seen to be reasonably smooth. We therefore assign the name Track III to it and exhibit it as the third principal track in Table X.

That this track disappears somewhere near 146 Mev can again be understood from Ashkin diagrams using positive pions alone: As we have seen Track III corresponds to essentially the same π^+ scattering as Track I and therefore to the same (positive) Ashkin diagram. However, as we discussed in connection with the 217-Mev analysis, solution III arises from the point a_2 on the Ashkin diagram whereas solutions I and II arise from the point a_1 . As will be discussed in Sec. 9, the

TABLE X. Track III.

Energy (Mev)	α_2	α_1	α_{33}	α_{31}	α_{13}	α_{11}
217	-67	0	40	37	4	-11
194	-43	1	58	23	5	-19
169	-42	7	49	12	1	2

³¹ Or T1a since at this energy Tracks T1 and T1a are indistinguishable.

Ashkin solution a_2 exists only when the total cross section is reasonably close to the resonance cross section $8\pi\lambda^2$ which is the case only in a limited energy region approximately from 150 Mev to 200 Mev. At 120 Mev, a_2 is definitely excluded and, since the $T=\frac{1}{2}$ phase shifts are small, only two solutions are present. Therefore, since Track III is associated with the point a_2 it must disappear somewhere above 120 Mev, namely, at the point where a_2 is no longer admissible. Whether this point be 146 Mev or another energy is not pertinent to our argument.

The "first" solution of Fermi and Metropolis reported in the preceding paper follows essentially Track III at high energies and Track I at low energies. It can again be shown by use of Ashkin diagrams (Sec. 9) that the solutions of Tracks I and III become identical at some energy if only positive mesons are considered; in other words, that Tracks I and III cross. One is therefore free to go from one track to the other without a discontinuity in phase shifts; but there will, of course, be a discontinuity in first derivative. If data for π^+ scattering existed and if they were very accurate, then the decision between these tracks could be made on this basis: If the Track I solution were correct, then the solution using Track I at low and Track III at high energy would show a definite break in the curve of phase shifts vs energy, particularly for α_3 . However, the availability of only negative-pion data with rather large experimental error, plus the possibility of taking up slack in the phase shifts α_{11} and α_{13} , made it possible for Fermi and Metropolis to obtain a rather smooth curve for all six phase shifts vs energy using a combination of Tracks I and III.

There is at present no experimental argument to disprove the Fermi-Metropolis set. However, since Ashkin's point a_2 nearly disappears at 217 Mev, we expect that accurate angular distribution measurements at slightly higher energies (260-300 Mev) will definitely discriminate between Tracks I and II on the one hand and Track III on the other. Because of the physical arguments which we shall give later (Sec. 10), we believe that the combination of Tracks I and III is not the correct solution.

We are thus left with Tracks I and II. The coefficients A_- , B_- , C_- , A_0 , B_0 , and C_0 of Tracks I and II

coincide with the mean input coefficients by construction.

The π^+ predictions of Tracks I and II for C_+ are shown in Fig. 3. Track I points are shown as little squares and Track II points as little triangles. It will be noted that neither set of points is in sharp disagreement with experiment except for C_+ as deduced from measurements at 188 Mev. For the time being the reader should ignore the curves; we shall discuss their meaning in Sec. 7. The calculated values for A_+ are in good agreement with experiment but for B_+ the calculated value is generally higher than the observed. The most apparent discrepancy is in the predicted B_+ at 217 Mev compared to the measured Brookhaven value at 225 Mev. We shall discuss in Sec. 7 why this is probably not too serious.

The predicted total π^+ cross section of Track I seem to be in very good agreement with the Carnegie experimental data as plotted in Fig. 2. Since these are much better than the angular distributions of π^+ , we regard the disagreements with the latter as not serious.

6. SENSITIVITY OF RESULTS

So far the solutions have been obtained with the mean values of the input data as given in Table I. To test the sensitivity of the results to the changes in the input coefficients it was decided to adopt the following procedure at 144, 194, and 217 Mev.

The MANIAC was started off with the solution of Track I at 217 Mev. Then each input coefficient was varied upward and downward roughly to the limit of

the experimental error shown in Table I. At the same time the other five input coefficients were kept at their mean value. A new solution was thereby found, showing the effect of changing this one input coefficient. The results of this operation are shown in Tables XI(a) and XI(b).

In Table XI(a) we show first the original solution for ease of reference. In the next line the case where A_- was varied so as to be a smaller number is shown. By leaving blank the values in the columns A_0 through C_0 we mean to imply that these values are essentially unchanged from the original (occasionally one of the other coefficients also varies by 1-2 percent of its original value). We repeat this procedure, varying A_- upward, and then do it in turn for the other coefficients. In Table XI(b) we show the resultant values of A_+ , B_+ , and C_+ and also list $\sigma_T(\pi^+)$ and $\sigma_T(\pi^-)$ for easy reference. In a few cases the variation of $\sigma_T(\pi^-)$ is more than the ± 2 mb permitted by the transmission experiments. More significant are the variations of the resultant $\sigma_T(\pi^+)$: the interpolation between the better measurements of $\sigma_T(\pi^+)$ on Fig. 2 exclude variations of "A₀ down" and "C₀ down" to the full limit of error for these quantities. The most striking feature of Table XI(a) is that it shows the sensitivity of the coefficients α_{13} and α_{11} : their values apparently cannot be determined with any reliability. On the other hand, the principal phase shifts seem to be rather insensitive to permissible changes of the input coefficients.

Next it was thought desirable to investigate the variation of more than one coefficient at a time. Natu-

TABLE XI. Input variation. 217 Mev, Track I.

	A_-	A_0	B_-	B_0	C_-	C_0	α_0	α_1	α_{11}	α_{13}	α_{15}	α_{17}
Original	0.13	0.20	0.12	0.19	0.37	0.75	-20	-4	107	-14	7	-7
A_- down	0.110						-21	-3	105	-12	-1	-2
A_- up	0.148						-21	-5	106	-11	9	-8
A_0 down		0.169					-17	-4	120	-20	12	-14
A_0 up		0.229					-23	-3	95	-12	-1	0
B_- down			0.089				-18	-2	108	-15	9	-9
B_- up			0.151				-22	-6	105	-13	3	-3
B_0 down				0.155			-19	-5	104	-13	4	-5
B_0 up				0.228			-21	-3	110	-15	8	-9
C_- down					0.312		-22	-7	108	-9	4	1
C_- up					0.433		-19	-2	107	-10	7	-12
C_0 down						0.626	-17	-3	122	-18	13	-16
C_0 up						0.854	-22	-8	105	-16	3	10

	A_+	B_+	C_+	$\sigma_T(\pi^+)$	$\sigma_T(\pi^-)$
Original	0.855	0.956	3.46	160	56.0
A_- down	0.916	0.931	3.35	162	54.4
A_- up	0.869	0.980	3.47	161	57.6
A_0 down	0.500	0.983	3.62	136	53.6
A_0 up	1.07	0.927	3.34	174	58.4
B_- down	0.791	0.859	3.49	156	56.1
B_- up	0.941	1.03	3.37	165	55.9
B_0 down	0.909	0.845	3.40	163	56.0
B_0 up	0.797	1.08	3.49	156	56.1
C_- down	0.942	1.01	3.10	157	53.9
C_- up	0.785	0.933	3.73	161	57.7
C_0 down	0.497	0.966	3.35	129	52.7
C_0 up	0.893	1.08	3.61	167	58.7

TABLE XII. Input variation. 217 Mev, Track I.

	A_-	A_0	B_-	B_0	C_-	C_0	α_3	α_1	α_{33}	α_{31}	α_{13}	α_{11}
Original	0.13	0.20	0.12	0.19	0.37	0.75	-20	-5	107	-14	7	-8
Case 1	0.109	0.168			0.433	0.874	-19	-3	104	-20	4	-6
2	0.148	0.232			0.306	0.630	-23	-8	111	-5	10	-6
3	0.110				0.433		-20	-1	105	-16	3	-9
4	0.148				0.310		-23	-9	107	-8	7	1
5		0.168				0.873	-21	-6	106	-18	6	-3
6			0.151	0.229			-23	-5	108	-14	6	-7
7			0.0892	0.154			-18	-4	105	-14	7	-8
8			0.0891	0.228			-19	-1	112	-17	11	-11
9	0.110		0.0891	0.228	0.433		-19	2	111	-19	7	-12
10		0.232	0.0891	0.228		0.626	-19	0	116	-15	12	-15
21	0.122	0.207	0.136	0.243	0.361	0.776	-25	-4	103	-12	1	3
22	0.152	0.183	0.147	0.155	0.339	0.814	-23	-12	107	-13	2	8
23	0.152	0.215	0.147	0.155	0.404	0.807	-23	-12	98	-17	0	8

	A_+	B_+	C_+	$\sigma_T(\pi^+)$	$\sigma_T(\pi^-)$
Original	0.855	0.959	3.456	160	56.0
Case 1	0.777	0.934	3.968	168	56.9
2	0.957	1.053	2.842	152	55.2
3	0.831	0.925	3.635	163	56.1
4	0.965	1.078	3.072	159	55.9
5	0.812	1.004	3.725	164	56.8
6	0.867	1.169	3.443	161	56.0
7	0.855	0.756	3.456	160	56.0
8	0.709	0.961	3.546	151	56.0
9	0.691	0.945	3.763	155	56.1
10	0.664	0.952	3.290	141	55.3
21	0.978	1.157	3.404	168	56.5
22	0.899	1.091	3.366	161	57.4
23	0.979	1.021	3.631	175	61.6

rally a great many variations are possible. However, of these, certain ones play havoc with the resultant $\sigma_T(\pi^-)$ and $\sigma_T(\pi^+)$ cross sections and were, therefore, excluded. Certain other variations merely change $\sigma_T(\pi^-)$ a little more than the allowable ± 2 mb. Of the combined variations, cases 21, 22, and 23 were devised with the intent to maximize the change of one or the other of the phase angles.

All the results are shown in Tables XII(a) and XII(b), with the same conventions as those adopted for Tables XI(a) and XI(b). It will be noted that in first approximation the effect of varying more than one coefficient at a time is additive in terms of the effect on the angles, except insofar as α_{11} and α_{13} are concerned.

Table XII(a) and XII(b) show several features. First, it does not seem possible to make α_{31} change sign. This is relevant because there is some evidence that α_{31} is positive around 100 Mev. The same seems to be true of α_1 . The phase angle α_3 is rather well established and not very sensitive. The phases α_{13} and α_{11} cannot both be simultaneously made zero, judging from the variations we tried. Changes of α_{33} up to $\pm 9^\circ$ are possible but in these cases [Eqs. (10) and (23)] the total cross section $\sigma_T(\pi^+)$ changes substantially so that the Carnegie measurements of $\sigma_T(\pi^+)$ determine α_{33} very accurately.

Variations of single coefficients for Track I at 144 Mev are shown in Tables XIII(a) and XIII(b). From Table XIII(b) we see that probably the full

variations of A_0 down, C_0 down, and C_0 up can be excluded on the basis of $\sigma_T(\pi^+)$. The most interesting result of Table XIII(a) is the instability of α_3 at this energy, and the high stability of α_{33} , especially when large changes of $\sigma_T(\pi^+)$ are excluded.

Variations of more than one coefficient at a time were also carried out for Track I at 144 Mev. The results are given in Tables XIV(a) and XIV(b). Of these, case 34 was set up with the specific intention to lower the somewhat high value of α_1 . It will be seen that indeed α_1 can be lowered quite markedly, namely from 13 to 9° . While the values of α_{11} and α_{13} are not too big we still did not find a variation which gave $\alpha_{11} = \alpha_{13} \approx 0$ and α_1 less than 12° .

Input variations of one coefficient at a time were also carried out at 194 Mev for Track I. The phase shifts showed appreciably greater sensitivity but not quite as great as we anticipated for this critical energy region. However, in a few of these variations the resulting solutions had a very large M value [Eq. (23)]. This meant that the phase angles, which the computer obtained as a solution, led to A_- , B_- , C_- , A_0 , B_0 , and C_0 different from the mean input values, apart from the one that was purposely changed. We believe this to indicate that these particular input changes do not permit a solution in the neighborhood of Track I. This was in particular the case when B_0 or C_0 was increased to its experimental limit. In both cases a solution could be found only if at the same time C_- was increased even

TABLE XIII. Input variation. 144 Mev, Track I.

	A_-	A_0	B_-	B_0	(a)							
					C_-	C_0	α_3	α_1	α_{33}	α_{31}	α_{13}	α_{11}
Original	0.0900	0.120	0.0800	-0.210	0.170	0.430	-13	14	46	5	3	-5
A_- down	0.0704						-12	13	46	5	1	-4
A_- up	0.109						-15	13	47	5	4	-8
A_0 down		0.0774					-12	12	41	10	5	-10
A_0 up		0.170					-19	13	50	1	1	-4
B_- down			0.0488				-9	14	47	4	2	-5
B_- up			0.107				-20	10	45	7	4	-8
B_0 down				-0.250			-8	11	49	3	2	-4
B_0 up				-0.159			-20	13	44	8	4	-8
C_- down					0.119		-11	13	46	3	1	-7
C_- up					0.220		-16	12	47	7	4	-5
C_0 down						0.244	-23	14	37	4	6	-4
C_0 up						0.617	-7	13	57	8	-1	-10

	A_+	B_+	C_+	$\sigma_T(\pi^+)$	$\sigma_T(\pi^-)$
Original	0.494	-0.381	1.843	143	52.9
A_- down	0.465	-0.362	1.805	138	50.3
A_- up	0.435	-0.396	1.882	138	55.4
A_0 down	0.307	-0.390	1.907	122	47.4
A_0 up	0.669	-0.364	1.805	165	59.3
B_- down	0.500	-0.480	1.869	146	52.9
B_- up	0.483	-0.288	1.818	141	52.9
B_0 down	0.449	-0.504	1.882	148	52.9
B_0 up	0.532	-0.219	1.818	140	52.9
C_- down	0.498	-0.305	1.651	136	50.7
C_- up	0.485	-0.438	1.997	149	55.0
C_0 down	0.444	-0.521	1.267	120	44.9
C_0 up	0.492	-0.232	2.330	165	60.9

beyond its experimental limit. Thus if a more accurate measurement gave values of B_0 and C_0 near the present upper experimental limit, and if at the same time C_- were left unchanged, then there would probably be no solution near Track I. Apart from this, an exact phase shift determination at this energy would require particularly precise knowledge of the experimental angular distributions.

For the Yang track, Track II, the variation was carried out for single coefficients only and only at 144 Mev. Again (as in the case of Track I) α_3 is very sensitive, while α_{33} and α_{31} are not.

7. INTERPOLATION OF PHASE ANGLES

From the discussion so far, it is evident that we have more reason to believe the results of Tracks I and II at 120 Mev, 144 Mev, and 217 Mev than at the intermediate energies between 144 and 217 Mev. The experimental data are more accurate at the lowest and highest energy; on the other hand, the phase shifts are less sensitive to the experimental data than at the intermediate energies. It is, therefore, perhaps more reasonable to obtain the phase shifts at the intermediate energies by interpolation of the phase shifts between 120 (or 144) and 217 Mev rather than by actual analysis

TABLE XIV. Input variation. 144 Mev, Track I.

	A_-	A_0	B_-	B_0	(a)							
					C_-	C_0	α_3	α_1	α_{33}	α_{31}	α_{13}	α_{11}
Original	0.0900	0.120	0.0800	-0.210	0.170	0.430	-14	13	47	5	3	-6
Case 11		0.0699				0.678	-6	12	44	19	2	-1
12		0.143				0.307	-19	14	42	2	4	-4
31		0.169	0.111	-0.160	0.121	0.415	5	18	46	-1	-9	1
32		0.0684	0.111	-0.160	0.120	0.675	5	17	44	12	-5	-11
34			0.0488	-0.159			-12	9	48	3	2	-6
35		0.170	0.0486	-0.159	0.119		-9	11	51	-5	-3	-5

	A_+	B_+	C_+	$\sigma_T(\pi^+)$	$\sigma_T(\pi^-)$
Original	0.494	-0.381	1.843	143	52.9
Case 11	0.192	-0.224	2.637	138	57.1
12	0.554	-0.465	1.459	134	50.6
31	0.520	0.171	1.507	132	56.4
32	0.298	0.214	2.159	132	54.6
34	0.546	-0.322	1.834	149	52.9
35	0.715	-0.210	1.587	125	57.1

TABLE XV. Values of α_{33} for interpolation (b) of Sec. 7.

Mev	α_{33}
120	30.0°
127	34.0°
133	38.1°
139	42.5°
144	46.0°
151	51.5°
160	58.8°
169	66.5°
178	73.9°
184	78.9°
188	82.5°
194	87.5°
202	94.3°
208	99.4°
217	107.0°

of the experimental data. It is encouraging for such interpolation that Track I shows already an almost linear behavior for α_{33} between 120 and 217 Mev. Similarly, if the values of α_3 are plotted against the momentum of the meson (in the center-of-mass system) and if a straight line is drawn on this plot between the values (Track I) of α_3 at 120 and 217 Mev, then this line will also fit the experimental data at energies below 120 Mev down to 60 Mev.

In view of the above, we tried the following interpolations:

(a) All phase angles linearly interpolated between the Track I values at 120 and 217 Mev.

(b) Between 120 and 217 Mev, Track I values, α_1 parabolically interpolated with zero slope at 120 Mev,³² α_{33} read off from a smooth plot of Track I points as given in Table XV, other 4 phase angles linearly interpolated.

(c) Between 144 and 217 Mev, Track I, all phase angles linearly interpolated.

(d) Between 144 and 217 Mev, case 34 phase angles (table 14a) at 144 Mev and Track I phase angles at 217 Mev, all phase angles linearly interpolated.

(e) Between 144 and 217 Mev, Track II, all phase angles linearly interpolated.

(f) Between 144 and 217 Mev, Track IIa, all phase angles linearly interpolated.

Of these interpolations, we consider (b) the most useful one in that it comes closest to reproducing the experimental data. The more straightforward interpolation (a) gave values for B_- which were extremely low at all intermediate energies between 120 and 217 Mev; this was the reason for choosing interpolation (b). The results of interpolation (b) for the coefficients A , B , C are shown in Table XVI. For the $T = \frac{3}{2}$ phase shifts we have also extrapolated their behavior beyond 217 Mev by means of straight lines and computed A_+ , B_+ , and C_+ . These are also shown in Table XVI. The extrapolation to higher energies was not carried out for the coefficients involving $T = \frac{1}{2}$ phase shifts since α_1 is changing so rapidly in the region around 200 Mev, and it is difficult to predict its behavior beyond 200 Mev. The results of interpolation (b) are also shown graphically by means of a solid curve in Figs. 3 through 6. Furthermore, the total cross sections have been computed for interpolation (b) and are shown as solid curves on Figs. 1 and 2.

The coefficients A_0 , A_+ , C_0 , and C_- are given very well by interpolation (b) except for C_- at 169 Mev which is slightly outside experimental error. All other points for A_0 , A_+ , C_0 , and C_- are well within the experimental error. The calculated values for B_0 tend to be slightly too high, those for B_- appreciably too low; the latter quantity will be discussed in more detail below. The erratic behavior of A_- which is found experimentally is not reproduced by interpolation (b). This discrepancy of A_- at 169 Mev and B_- at 144 Mev are the only disagreements with the negative pion scattering data worth considering; at other energies A_- agrees well within and B_- is just at the limit of the experimental error.

TABLE XVI. Phase angle interpolation (b) of Sec. 7.

Mev	A_-	A_0	A_+	B_-	B_0	B_+	C_-	C_0	C_+
120	0.038	0.050	0.200	0.026	-0.150	-0.360	0.090	0.250	1.040
127	0.055	0.064	0.289	0.027	-0.147	-0.366	0.110	0.270	1.167
133	0.066	0.081	0.371	0.029	-0.152	-0.375	0.126	0.306	1.322
139	0.082	0.100	0.476	0.026	-0.144	-0.368	0.148	0.334	1.477
144	0.094	0.115	0.559	0.022	-0.138	-0.356	0.155	0.367	1.606
151	0.111	0.140	0.684	0.021	-0.120	-0.315	0.184	0.406	1.812
160	0.132	0.172	0.836	0.021	-0.090	-0.227	0.219	0.470	2.117
169	0.149	0.200	0.965	0.020	-0.045	-0.094	0.252	0.526	2.395
178	0.158	0.221	1.055	0.020	0.013	0.080	0.287	0.581	2.667
184	0.159	0.231	1.086	0.025	0.047	0.206	0.306	0.617	2.841
188	0.160	0.233	1.090	0.029	0.071	0.290	0.321	0.640	2.956
194	0.155	0.235	1.083	0.039	0.104	0.426	0.337	0.672	3.100
202	0.149	0.230	1.034	0.063	0.149	0.641	0.357	0.711	3.287
208	0.143	0.220	0.977	0.082	0.171	0.776	0.364	0.731	3.369
217	0.130	0.200	0.860	0.120	0.190	0.960	0.370	0.750	3.460
225			0.731			1.097			3.456
232			0.617			1.194			3.402
241			0.472			1.277			3.245

³² This horizontal tangent is indicated from our own analysis and also fits well with the values of α_1 known between 60 and 120 Mev.

For the positive pion scattering, disagreement at 151 Mev is not too bad. At 188 Mev the predicted values of both B_+ and C_+ are very much higher than the center of the observations but if the angular distribution is computed from our A_+ , B_+ , and C_+ of interpolation (b) and compared with the experimental points the agreement is well within the limits of error except at 45° . At 225 Mev the predicted value for C_+ , 3.46, agrees very well with the measured value of 3.8, the measured value now lying above the prediction. The predicted value for B_+ , 1.10, is considerably higher than the measured 0.44 but this discrepancy is probably not serious for two reasons. First, it is more difficult to deduce B_+ from the measurements than any other coefficient because the measured distribution does not

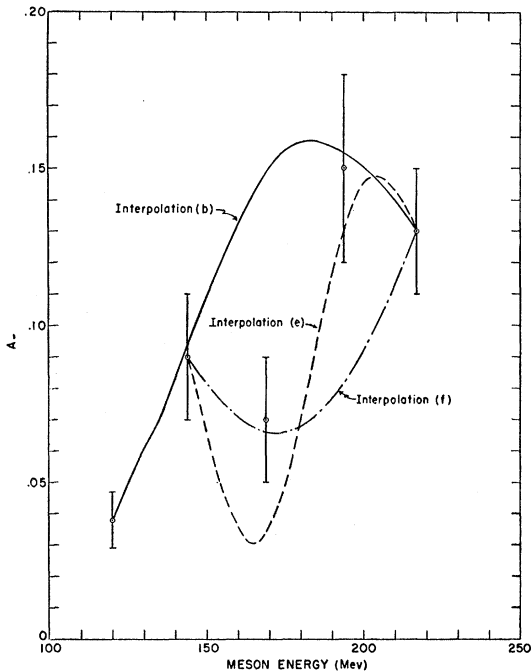


FIG. 4. The coefficient A_- of Eq. (3) as a function of energy. The curves are interpolations discussed in Sec. 7.

fit an expression of the form (2) very well. Second, the coefficient B_+ , in contrast to A_+ and C_+ , varies in a complicated way with energy; in fact, it must go through a maximum at some energy not far above 225 Mev (see, e.g., Fig. 11). Indeed, B_+ is given by

$$\frac{1}{2}B_+ = \sin\alpha_3 [2 \sin\alpha_{33} \cos(\alpha_{33} - \alpha_3) + \sin\alpha_{31} \cos(\alpha_{31} - \alpha_3)]. \quad (30)$$

If α_{31} is small, only the first term matters, and with $\alpha_3 \approx -20^\circ$, this term has a maximum for $\alpha_{33} \approx 125^\circ$. This behavior is shown by our extrapolation of B_+ : while B_+ decreases very much when the energy is decreased below 225 Mev, it does not increase much when it is raised. Hence, due to the wide energy spread of the mesons used in the Brookhaven experiments the average of B_+ should be lower than the value at 225 Mev.

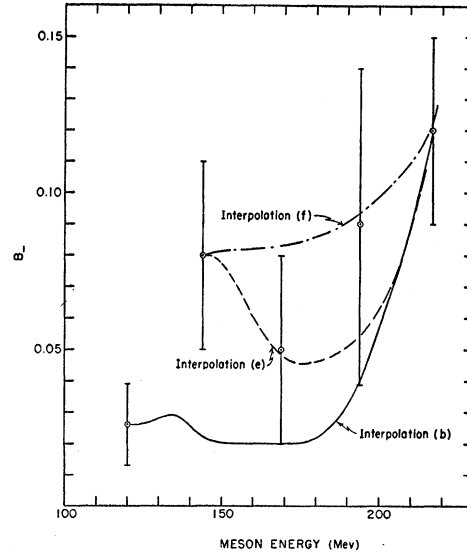


FIG. 5. The coefficient B_- of Eq. (3) as a function of energy. The curves are interpolations discussed in Sec. 7.

Perhaps the most striking behavior is exhibited by the coefficient B_- . In contrast to B_0 and B_+ , which change sign from negative at low to positive at high energies, B_- stays positive all the time. This is accomplished by the fact that the S scattering amplitude which is proportional to $(2\alpha_1 + \alpha_3)$ for π^- scattering itself changes sign from positive to negative. In fact, it is precisely the positive sign of B_- at 217 Mev which forces us to make α_1 zero or negative at this energy.

The tendency of the B coefficients to go through zero, however, still manifests itself in our predicted B_- by the fact that the predicted values stay small and almost constant over a large energy interval from about 100 to 180 Mev. To investigate this more closely, we note that the coefficient B_- is given by Eqs. (9), (17), and (18). In particular, if in first approximation we set $\alpha_{31} = \alpha_{13} = \alpha_{11} = 0$, then $y = b$. Furthermore, since α_3 and α_1 are small, we shall set $\sin\alpha_3 = \alpha_3$ and $\sin\alpha_1 = \alpha_1$. Then

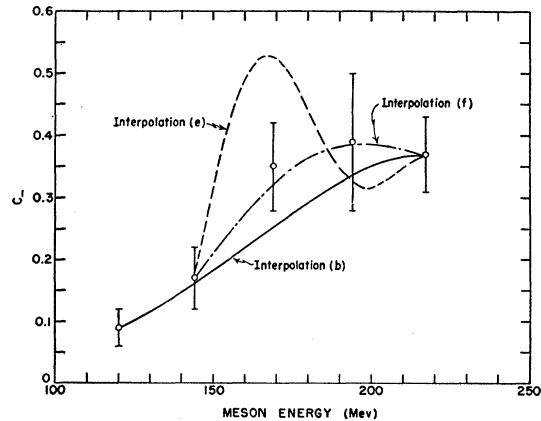


FIG. 6. The coefficient C_- of Eq. (3) as a function of energy. The curves are interpolations discussed in Sec. 7.

it can be shown that

$$B_- \approx (\alpha_3 + 2\alpha_1) \sin\alpha_{33} \cos\alpha_{33} + (\alpha_3^2 + 2\alpha_1^2) \sin^2\alpha_{33}. \quad (31)$$

The first term in Eq. (31), which is linear in α_3 and α_1 , is for this reason apt to be the larger. However, the coefficient $\cos\alpha_{33}$ goes through zero at the resonance which makes the term small. The first term would change sign if it were not for the fact that α_1 also changes sign in our energy interval. However, the fact remains that near the resonance only the second term in Eq. (31) survives and it is small of second order; this explains the small value of B_- .

The peculiar behavior of B_- would be a good test of our proposed solution for the phase shifts. More accurate experiments will be needed, and these might at the same time resolve the discrepancy for A_- at 169 Mev.

We now discuss our other interpolations: interpolation (c) gave somewhat similar results as interpolation (b) except that B_- has in this case a sharp peak at 145 Mev. The latter seems to be impossible because it is then very hard to connect with the 120-Mev point. Interpolation (d) gave essentially the same result as interpolation (c) but, because of the extreme phase angles chosen at 144 Mev, B_- started lower than for case (c) at 144 Mev; hence (d) is more similar to interpolation (b).

As to interpolations (e) and (f) we found the following: the true Yang Track II gives rather pronounced maxima and minima in the coefficients, A , B , C , as might be expected because of the very rapid variation of the Yang phase shifts. Track IIa gives quite smooth results for the coefficients and some of them are shown in Figs. 3 through 6. It is seen that a better experimental determination of A_- and B_- could well decide between Tracks IIa and I. The interpolated Track II phase shifts are shown to be unreasonable by the erratic curves for the A , B , C ; indeed, linear interpolation of the Yang phase shifts is not appropriate and does not, of course, rule out the Yang phase shifts as such because we know there is always a Yang set to every Fermi set if the α_{11} and α_{13} are small.

8. CONNECTION BETWEEN FERMI AND YANG SOLUTIONS

Among the solutions we have obtained, Track I gives by far the smoothest dependence of the phase shifts on energy. For this reason, and even more for the theoretical reasons to be discussed in Sec. 10, we believe it to be the correct solution. In this and the next section, we wish to discuss the relations between the various solutions. Further light will be thrown on these relations by the accompanying paper by R. L. Martin. We are very much indebted to Dr. Martin for many ideas which are presented in this and the next section; he pointed out to us first that the Fermi and Yang tracks for α_{33} must cross as shown in Fig. 7, and

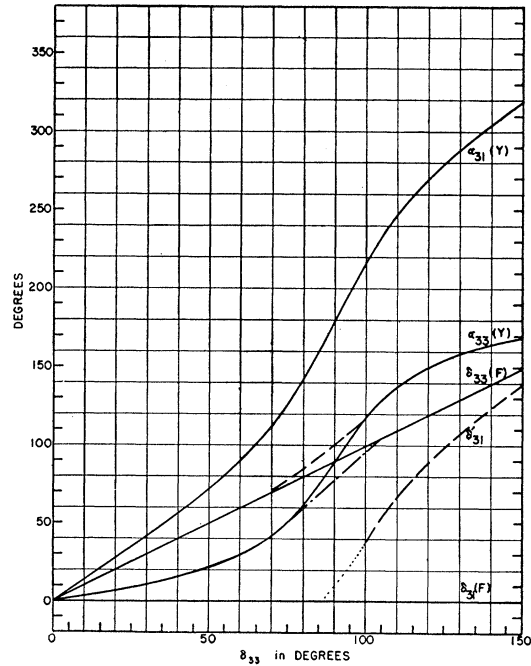


FIG. 7. The relation of the phase angles of Solutions I' (Fermi type) and II' (Yang type).

he gave us invaluable aid on the interpretation of Ashkin diagrams.

In our discussion, we shall consider the *positive* pion scattering as given. This is possible because, as we have repeatedly pointed out, all the acceptable solutions, Tracks I to III, give very nearly the *same* π^+ scattering. This in turn is due to the fact that α_{11} and α_{13} are small in all these solutions, and even α_1 is moderately small so that the π^- data can essentially be interpreted in terms of $T = \frac{3}{2}$ scattering with small corrections. Considering the π^+ scattering as given greatly simplifies the analysis.

Instead of starting from experimental data, we shall in this and the next section take the point of view that there is a "true" set of phase shifts very similar to Track I. We shall call it Track I'. Then from this true set we can calculate a π^+ angular distribution which we shall call the *theoretical distribution*. We shall then determine what other sets of phase shifts, if any, will also be compatible with the theoretical angular distribution; these we shall call "supplementary solutions."

We denote phase shifts in the "true solution" Track I' by δ instead of α and define them as follows: δ_{31} shall be zero for all energies, δ_{33} shall increase monotonically and fairly rapidly with energy, and δ_3 shall be negative and decrease slowly with energy. We shall not specify the relation between energy and phase shifts but merely the relation between the two non-vanishing phase angles, which we shall take to be

$$\delta_3 = -10^\circ - 0.1\delta_{33}. \quad (32)$$

This is rather well fulfilled by the original Track I in our energy range.

The "true solution" is of the Fermi type and we shall first investigate the Yang solution corresponding to it; the Yang phase shifts will be denoted by α . By definition the Yang solution has the same S phase as the Fermi solution, hence

$$\alpha_3 = \delta_3. \quad (33)$$

The difference between the $P_{\frac{1}{2}}$ and $P_{\frac{3}{2}}$ phase shifts is reversed, so that

$$\alpha_{31} - \alpha_{33} = \delta_{33} - \delta_{31} = \delta_{33}. \quad (34)$$

Finally the amplitude for P scattering without spin flip is preserved, i.e., [see Eq. (15)]

$$b \equiv 2(e^{2i\alpha_{33}} - 1) + e^{2i\alpha_{31}} - 1 = 2(e^{2i\delta_{33}} - 1). \quad (35)$$

Together with Eq. (34), this yields

$$e^{2i\alpha_{33}} = (2e^{i\delta_{33}} + e^{-i\delta_{33}}) / (2e^{-i\delta_{33}} + e^{i\delta_{33}}). \quad (36)$$

It is obvious that the right-hand side has absolute value unity so that a solution α_{33} exists, and it is easily seen that

$$\tan \alpha_{33} = \frac{1}{3} \tan \delta_{33}. \quad (37)$$

For small δ_{33} , Eq. (37) gives

$$\alpha_{33} \approx \frac{1}{3} \delta_{33}, \quad (38)$$

i.e., a small 33-phase, and then Eq. (34) yields $\alpha_{31} = (4/3)\delta_{33}$. As δ_{33} approaches 90° , however, α_{33} will also approach 90° : With our particular choice of the "true" Fermi solution, the Yang solution will have a $P_{\frac{3}{2}}$ resonance at exactly the same energy as the Fermi solution. The only difference is that the Yang phase passes through 90° much faster than the Fermi phase. This is illustrated in Fig. 7 which shows the Yang phase shifts α_{33} and α_{31} as functions of the Fermi phase δ_{33} . As δ_{33} approaches 180° , so does α_{33} , only faster.

The $P_{\frac{1}{2}}$ phase shift α_{31} changes much faster still. We have

$\alpha_{31} = (4/3)\delta_{33}$	90°	180°	270°	360°
when $\delta_{33} = \text{small}$	60°	90°	120°	180°

This is also given in Fig. 7. Thus, where the Fermi phase shifts show one resonance only, $\delta_{33} = 90^\circ$, the Yang shifts show three, one in α_{33} and two in α_{31} (90° and 270°). Somewhat surprisingly, these three resonances give exactly the same angular distribution at every energy as the one Fermi resonance so that the two solutions cannot be distinguished by experiment. However, the Fermi solution is far simpler and hence preferable unless there are strong theoretical arguments to the contrary. The similarity of the Yang solution to Track II is obvious. In particular, when $\delta_{33} = 107^\circ$ (which corresponds to 217 Mev on Track I) then Fig. 7 gives $\alpha_{33} = 133^\circ$ and $\alpha_{31} = 240^\circ$ which agree closely with the Track II values (Table VIII).

One important feature of our two solutions, Fermi

and Yang, is that the curves α_{33} and δ_{33} cross. With our choice of $\delta_{31} = 0$, this happens exactly at $\delta_{33} = 90^\circ$, and thus at $b = -2$, Eq. (35). In other words, for crossing to occur, the real part of b must have a specific value, -2 , when the imaginary part vanishes. If b is derived from experimental data, rather than from our "true solution," this will in general not be fulfilled, and then the crossing will not occur. Therefore, if we start from experimental data, it may appear more natural to join the curve α_{33} at large phase angles to the curve δ_{33} at small phase angles, and vice versa. This is indicated by the dashed and dot-dashed connecting lines on Fig. 7. In other words, what we call the Yang solution at high energies is then joined to the Fermi solution at low ones (dashed connection). We shall denote this combination as Track I'-II' and its phase angles by δ' . The δ_{31}' corresponding to this solution is zero at low energy and it is easy to see that continuity requires us to choose $\delta_{31}' = \alpha_{31} - \pi$ at high energies; then $\delta_{31}' < \delta_{33}'$, throughout as for a Fermi solution. The curve for δ_{31}' is also shown in Fig. 7, by a dashed line. It rises suddenly and rapidly from zero to high values. The exact behavior of δ_{31}' at the start from zero depends on the precise way how the lower and upper parts of the δ_{33}' curve are joined; to indicate the uncertainty of this beginning, it is shown dotted on Fig. 7. The behavior of δ_{31}' is of course physically very unreasonable. However, on purely experimental grounds, the primed solution cannot be excluded. The δ' solution will be further discussed in the accompanying paper by Martin.

9. THE FERMI-METROPOLIS SOLUTION

Ashkin and Vosko⁶ have pointed out that there are in general four solutions to the π^+ phase shifts rather than merely the Fermi and Yang solutions. To understand the other two solutions, we use Ashkin diagrams explicitly. We again consider positive pions only, and assume that there is a "true solution," defined as in the last section.

In the Ashkin-Vosko theory, we start from the amplitude for scattering without spin flip,

$$a + b \cos \theta, \quad (39)$$

where b is given by Eq. (35) and

$$a = e^{2i\alpha_3} - 1 \quad (40)$$

from Eq. (14). Ashkin and Vosko show that the experimental data on π^+ give (1) the quantity $|a+b|$, (2) the real part of $a+b$, and (3) the quantity $|a-b|$. The analysis then proceeds in four steps (see Fig. 8), viz.,

1. $a+b$ is determined by the experimental data (except for the sign of its imaginary part). The point $\frac{1}{2}(a+b)$ is plotted on a graph; we shall call it point P .
2. A circle is drawn around point P with radius $\frac{1}{2}|a-b|$. A fixed circle is also drawn around the point -1 with radius 1; we shall call it the a circle. The intersection of the two circles determines the point a . There are in general two intersections, a_1 and a_2 .

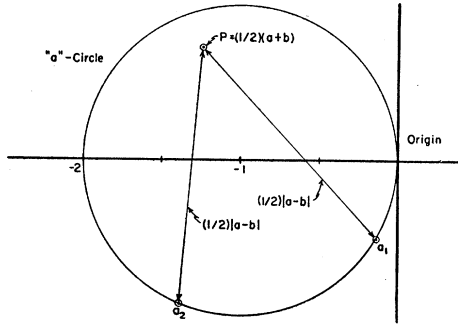


FIG. 8. Typical Ashkin diagram constructed from positive scattering coefficients A_+ , B_+ , and C_+ .

3. From $a+b$ and a , b is determined. By Eqs. (15) and (24), b must satisfy the inequality

$$|b+3| < 3. \quad (41)$$

Sometimes one of the solutions, a_2 , is ruled out by this inequality. We must also have from Eqs. (15) and (24):

$$|b+3| > 1. \quad (41a)$$

4. From b , the phase shifts α_{31} and α_{33} are found, using Eq. (15).

We shall construct the point $\frac{1}{2}(a+b)$ and determine $|a-b|$, not from experimental data, but from our "true solution." Thus we set

$$a = e^{2i\delta_3} - 1, \quad (42)$$

$$b = 2(e^{2i\delta_{33}} - 1) \quad (43)$$

where δ_3 and δ_{33} are considered *known* quantities. We then proceed with the Ashkin and Vosko method to find *all* solutions corresponding to the same "experimental data." Clearly, as we proceed to find the intersections of the two circles according to step 2 of the Ashkin and Vosko procedure, one of the intersections will be exactly the "input a " of Eq. (42); we shall call it a_1 and thus have the first solution,

$$a_1 = a, \quad b_1 = b. \quad (44)$$

This solution satisfies condition (41) by construction, and leads to the Fermi and Yang solutions discussed in the last section.

The other solution, a_2 , can then be found and examined as to whether it satisfies the inequality (41). To facilitate this, we shall for the moment simplify our assumed "true solution" still further by assuming $\delta_3 = 0$. Then the point P will lie on the a circle itself, at an angle $2\delta_{33}$ from the center. The point a_1 is now at the origin, and hence, as can be seen by suitable modification of Fig. 8, the point a_2 is by symmetry at the angle $4\delta_{33}$ on the a circle. Therefore,

$$a_2 = e^{4i\delta_{33}} - 1, \quad (45)$$

and the corresponding phase shift is

$$\alpha_3 = 2\delta_{33}. \quad (46)$$

Further,

$$b_2 = a + b - a_2 = 2e^{2i\delta_{33}} - e^{4i\delta_{33}} - 1, \quad (47)$$

and

$$|b_2 + 3|^2 = 9 + 4(\cos 2\delta_{33} - \cos 4\delta_{33}) \leq 9. \quad (48)$$

Thus we must have

$$\cos 2\delta_{33} < \cos 4\delta_{33}, \quad (49)$$

which is satisfied if and only if

$$60^\circ < \delta_{33} < 120^\circ. \quad (50)$$

In other words, the solution a_2, b_2 is not admissible if the "true" phase shift δ_{33} is small; in this region, there are only two solutions to our artificial problem, the Fermi and the Yang. When the true δ_{33} exceeds 60° , a new solution a_2 appears which is characterized by the large and rapidly varying phase shift α_3 given by Eq. (46). This solution will disappear again when δ_{33} reaches 120° . Thus the new solution can exist only if the cross section is large, in fact fairly close to the resonance cross section. Trouble with the phase shift analysis is, therefore, expected to arise, and in practice does arise, only in the region of large cross section. This fact has been mentioned already in Sec. 5.

In general, for any given value of δ_{33} , there will be two solutions belonging to a_2 , of the Fermi and the Yang types, but at the points where the solution a_2 just appears or disappears, there will be only one set α_{33}, α_{31} because $|b+3|$ is exactly 3. This is the reason why there is only one solution of this type at 217 Mev, as shown in Sec. 4a.

If we start from low energies and thus from low δ_{33} , the solution a_2, b_2 will at first not exist, and when it first appears it has completely different values of all phase shifts, *viz.*,

$$\alpha_3 = 120^\circ, \quad \alpha_{33} = 30^\circ, \quad \alpha_{31} = 30^\circ,$$

as compared with the "true" solution,

$$\delta_3 = 0, \quad \delta_{33} = 60^\circ, \quad \delta_{31} = 0.$$

Therefore, no transition can be made at this point from the δ solution to the α solution. However, as δ_{33} (and the energy) increases, the point a_2 moves around the a circle and finally reaches the origin when $\alpha_3 = 180^\circ$. This suggests a change in the definition to

$$\alpha_3' = \alpha_3 - \pi = 2\delta_{33} - \pi. \quad (51)$$

Then $\alpha_3' = \delta_3 = 0$ when $\delta_{33} = 90^\circ$. In fact, at this point *all* phase shifts of solution a_2 will agree with those of solution a_1 . Therefore, we may use the "true" solution a_1 up to this point, and then switch to solution a_2 , *without any discontinuity* in any of the phase shifts. This can be done either with the Fermi or the Yang set. After the switch is made, the phase α_3' will go from 0 to 60° .

We have still another alternative: it has been pointed out that the imaginary part of $a+b$ cannot be determined experimentally. It is, therefore, always possible

to replace the point P by its mirror image P' with respect to the real axis, this replaces δ_{33} by $\pi - \delta_{33}$, and changes the sign of all other phase shifts; α_3' is replaced by

$$\alpha_3'' = -\alpha_3' = \pi - 2\delta_{33}. \quad (52)$$

We can thus use the following solution: $\alpha_3 = 0$ for δ_{33} up to 90° , and α_3'' thereafter. The transition again involves no discontinuity in phase shifts. After the transition, the phase α_3'' goes from 0 to -60° ; then the solution disappears. The behavior of α_3 follows essentially our previous Track I at low energies and switches to Track III afterwards, as will become still clearer in the rest of this section. We shall, therefore, call this solution Track I'-III'.

We now make our discussion more realistic by returning to the original choice (32) for our "true" solution. For this case, we have calculated numerically the phase shifts corresponding to the a_2 solution and shown them in Fig. 9. Both the solutions α_3' and α_3'' are shown.³³ Their similarity with the simpler case discussed above will be clear. It is possible either to go from solution δ_3 at low energies to α_3' at high; then the transition occurs at the point $\delta_{33} = 66^\circ$ and α_3' goes to high positive values afterwards. Or the transition can be made from α_3 to α_3'' ; this transition occurs at $\delta_{33} = 81^\circ$ and α_3'' then goes to large negative values. This is essentially the behavior of the Fermi-Metropolis solution.

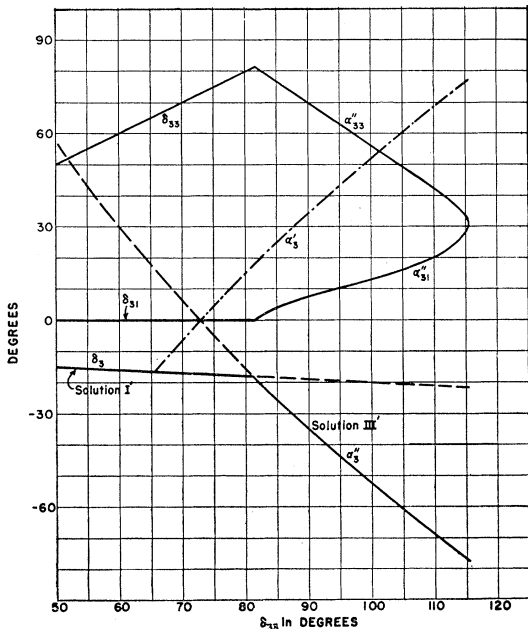


FIG. 9. The relation between the phase angles of Solution I' (Fermi type) arising out of the point a_1 and Solution III' (Fermi type) arising out of the point a_2 .

³³ Actually there is a very small region around $\delta_{33} = 75^\circ$ where the a_2 solution does not exist even though $|b+3| > 3$; in this region there is no solution because $|b+3| < 1$, which violates Eq. (41a).

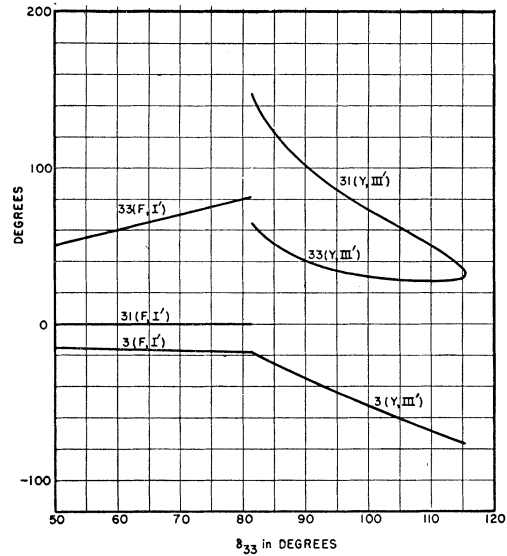


FIG. 10. Solution IV'; i.e., Solution I' (Fermi type) arises out of the point a_1 until $\delta_{33} = 81^\circ$ and Solution III' (Yang type) arises out of the point a_2 from then on.

We also give in Fig. 9 the calculated values of α_{33}'' and α_{31}'' which are derived from our "theoretical distribution" by taking the S phase shift to be α_3'' . Figure 9 gives the Fermi type phases, Fig. 10 the Yang type. The Fermi type phases are again very similar to those of the Fermi-Metropolis solution: α_{33} goes up to a high value (in our case 81°) then decreases to about 32° . The phase α_{31} is zero until α_{33} reaches its maximum, then it increases rapidly and becomes finally equal to α_{33} . At this point, the solution disappears.

The solutions of Fig. 9 have continuous phase shifts but discontinuities in the derivatives of the phase shifts with respect to energy. If the experimental data were infinitely accurate, and if they were to agree with our "theoretical distribution," then these discontinuities in derivative would show up and could be used to rule out the a_2 type solutions. At present, the inaccuracy of the experimental data smooths out the plot of phase shift vs energy, and this tendency is further helped if also the phase shifts α_1 , α_{13} , and α_{11} are available to fit the experimental data. Therefore, the Fermi-Metropolis solution was much smoother than our solution on Fig. 9 and did not show an actual discontinuity in derivative.

The Yang solution, Fig. 10, does not join to the low-energy Fermi solution at the transition point, $\delta_{33} = 81^\circ$, but there is in this case a discontinuity in value as well as derivative. The Yang solution corresponding to point a_2 would join smoothly to the low-energy Yang solution, Fig. 7. It is interesting that for the Yang solution given in Fig. 10, both α_{31}'' and α_{33}'' decrease with increasing energy (i.e., δ_{33}); they become equal to each other and to the phases of the Fermi solution, Fig. 9, when the solution a_2 disappears at $\delta_{33} = 115.5^\circ$. If one

tries to join the Yang solution of point a_2 to the *Fermi* solution of a_1 , then α_{31}'' of Fig. 10 should be replaced by $\alpha_{31}'' - 180^\circ$, but even then it joins very poorly. No solution has been found by the MANIAC which corresponds to Fig. 10 or any simple modification of it.

The Track III solution given in Sec. 5 follows Fermi and Metropolis at high energy, and then follows the α'' solution of Fig. 9 down to lower energies as well. This is the reason for the disappearance of Track III when the energy is decreased below 146 Mev. As has repeatedly been pointed out, it is not necessary to follow the α'' curve down to its disappearance at low energy but we may switch to Track I in the manner of Fermi and Metropolis.

What happens when the Track III solution disappears at high energy? We know from Sec. 5 that this essentially occurs at 220 Mev. If we go to any higher energy, and if our "theoretical distribution" remains valid there, then it can no longer be fitted by phase shifts which join continuously to the Track III solution at 220 Mev. Because of experimental errors, an approximate fit to the experimental data will remain possible for some time but ultimately the Track III solution will break down. This prediction is, of course, true only if our theoretical distribution really agrees with the experimental angular distributions of the future.

If we are correct in saying that Track III disappears at 220 Mev, then the near-equality of α_{31} and α_{33} at 217 Mev should be considered a danger sign. For the equality $\alpha_{31} = \alpha_{33}$ represents an extremum: $|b+3|$ has then its maximum value 3. To let α_{31} increase beyond

α_{33} does not help, but merely brings us into the domain of Yang solutions. The condition $\alpha_{31} = \alpha_{33}$ eliminates the spin flip term and thus helps to increase the anisotropy of the angular distribution: this is necessary in the Track III solution because the large α_3 provides a very large isotropic term by itself.

In Fig. 11, we illustrate the manner in which the breakdown of Track III might manifest itself. The figure is constructed as follows: we still assume that the "theoretical distribution" is the correct one. On the basis of the behavior of the phases when Track III disappears, we surmise that a Type III solution will approximate the angular distribution most closely if we assume $\alpha_{31} = \alpha_{33}$. With this assumption, we can then determine α_3 and α_{33} for an "extrapolated Track III" by requiring that A_+ and C_+ be correctly given thus:

$$\sin^2 \alpha_3 = A_+, \quad (53)$$

$$\sin^2 \alpha_{33} = C_+/9. \quad (54)$$

Then we can calculate B_+ ; it is

$$B_+' = 6 \sin \delta_3 \sin \delta_{33} \cos(\delta_{33} - \delta_3). \quad (55)$$

This "Track III value" of B_+' can then be compared with the correct value, B_+ of the theoretical distribution. The result is shown in Fig. 11: there is evidently no similarity at all between B_+ and B_+' . While B_+ still rises beyond the critical point, $\delta_{33} = 115^\circ$, B_+' falls sharply and even becomes negative at a somewhat higher energy. Even a rough measurement of the angular distribution at energies from about 250 to 350 Mev should make a decision between Tracks I and III possible.

10. CONTINUITY AND THEORY

We have seen that it is impossible, on the grounds of existing experiment alone to decide between the various "tracks." Possibly future experiments beyond 225 Mev will rule out Track I-III but so far these do not exist. We must therefore have recourse to more or less theoretical arguments.

Theoretically, the phase shifts must be analytic functions of the energy. This rules out sharp corners in the α vs E plot, and strongly favors a smooth variation. By far the smoothest variation of all the α 's with energy is provided by our Track I, and we regard this as a strong argument in favor of this track.

Track I-III, the Fermi-Metropolis solution, appears unlikely for the following reasons. First of all, the phase α_{31} which is very small up to about 160 Mev, suddenly starts to rise rapidly. While an actual break in the curve is avoided by suitable choice of the small phase shifts α_{11} , α_{13} , we still believe that it would be almost impossible to devise a theory to give just this behavior of α_{31} .

Stranger still is the behavior of α_3 . Apart from a complicated behavior at low energies,³⁴ this quantity up to

³⁴ R. E. Marshak, Phys. Rev. 88, 1208 (1952).

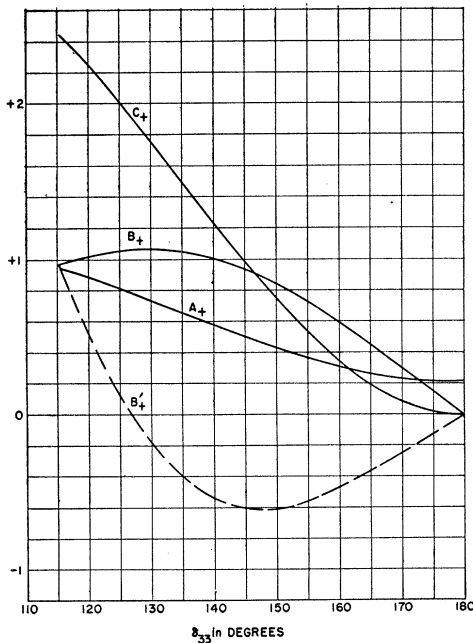


FIG. 11. The manner in which the breakdown of Track III might occur.

about 150 Mev behaves very regularly, being represented quite well by a straight line; in degrees, we have

$$\alpha_3 = 9.6^\circ - 17.1^\circ \eta, \quad (56)$$

where η is the meson momentum in units of μc in the center-of-mass system. Now this is what should be expected from a strong repulsive potential of short range (about $2\hbar/Mc$). Indeed, available theory, either using the Tamm-Dancoff method³⁵ or a contact transformation,³⁶ predicts just such a repulsion, arising from the virtual production of a nucleon pair. If this is correct, then a behavior like Eq. (56) should remain valid up to energies of the order Mc^2 . Quite generally, *any* strong repulsive potential will give a negative phase shift proportional to the momentum, and when the energy gets high enough to penetrate the repulsive core, the slope of the curve α vs η will become *smaller*. It seems almost impossible to construct a repulsive interaction in an *S* state which would make the α vs η curve suddenly much steeper at high energies.³⁷

The rather sharp peak of α_{33} in Solutions I-III also makes a theoretical explanation difficult, and in particular a close approach to 90° followed by a rapid decrease looks suspicious.

In Track II, α_3 is well-behaved, and also the monotonic increase of α_{33} and α_{31} with energy is reasonable. However, the extremely rapid increase of α_{33} and α_{31} , and the need to explain 3 resonances rather than 1, make this track also very unlikely.

The combination Track I and IIa or I'-II' (dashed line in Fig. 7) is rejected because of the sudden and rapid increase of α_{31} after δ_{33} passes 90° .

A Track Ia may be defined as follows: Below 194 Mev, it agrees with Track I; above 194, the signs of all

phase shifts are reversed, except for α_{33} which is replaced by $\pi - \alpha_{33}$. This in fact is the solution 1 of Table II which was found originally at 217 Mev. We reject this track mainly because of the sudden jump of α_3 from negative to positive values near 194 Mev, and also because α_{33} goes close to 90° and then falls again, with almost a break at the top.

Track I has no such faults and we therefore believe it to be the correct solution.

A further argument for Track I is the behavior of photomeson production, as analyzed by Ross.³⁸ Particularly the fact that the experimental angular distribution of positive photomesons shifts from a backward to a forward maximum at high energies, is strong evidence for a resonance in α_{33} . Watson³⁹ has given an argument for the same conclusion on the basis of the (less well measured) angular distribution of neutral photomesons.

As to the *theory* of meson scattering, the quantitative results of the Tamm-Dancoff theory are still very incomplete, and many points in the method are not yet well understood. However, some qualitative features seem clear, both from the nonrelativistic formulation of Chew⁷ and from the relativistic one of Dyson *et al.*⁷ These are: (1) only the phase α_{33} is large, due to an attractive interaction in this state; (2) α_{33} may (but does not need to) have a resonance; (3) α_{31} , α_{11} and α_{13} are small and slowly varying; and (4) α_3 behaves as if there were a strong repulsive potential of short range. Calculations of α_1 are complicated by renormalization problems, but a positive value is likely.

Track I or rather an interpolation like (b) in Sec. 7 is the only one which agrees with these theoretical predictions. Together with its smoothness, we believe this makes it almost certain that it is the correct one.

We should like to thank Josephine Powers for helping with the hand computing.

³⁵ Dyson, Ross, Salpeter, Schweber, Sundaresan, Visscher, and Bethe, Phys. Rev. (to be published).

³⁶ S. D. Drell and E. M. Henley, Phys. Rev. **89**, 1053 (1952).

³⁷ A long-range attractive potential plus a strong short-range repulsion will make the α vs η curve bend downwards, but this will occur mostly at low energy and certainly not set in suddenly.

³⁸ M. Ross, Phys. Rev. **94**, 454 (1954).

³⁹ K. M. Watson (private communication).